A tale of three types of internal object representations in the human brain

Shuang Tian[1,2], Xiaomin Mao[2], Rui Feng[2], Dahui Wang[1,2,3], Xiaoying Wang[2 #], Yanchao Bi[4,5,6,7,8,2 #]

Affiliations:

1 School of Systems Science, Beijing Normal University, Beijing, China, 100875

2 State Key Laboratory of Cognitive Neuroscience and Learning & IDG/McGovern Institute for Brain Research, Beijing Normal University, Beijing, China, 100875

3 Beijing Key Laboratory of Brain Imaging and Connectomics, Beijing Normal University, Beijing, China, 100875

4 School of Psychological and Cognitive Sciences and Beijing Key Laboratory of Behavior and Mental Health, Peking University, Beijing 100871, China

5 Institute for Artificial Intelligence, Peking University, Beijing 100871, China

6 IDG/McGovern Institute for Brain Research, Peking University, Beijing 100871, China

7 Chinese Institute for Brain Research, Beijing 102206, China

8 Key Laboratory of Machine Perception (Ministry of Education), Peking University, Beijing 100871, China

Correspondence to: Yanchao Bi (email: ybi@pku.edu.cn); Xiaoying Wang (email: wangxiaoying@bnu.edu.cn)

Abstract

Both object knowledge retrieval and sensory imagery generation engage perceptual regions in the brain and exhibit representational overlap with perception. However, whether these processes rely on common or distinct internal representations remains unclear. We conducted an fMRI visual working memory experiment in individuals with (visualizers) and without (aphantasics) visual imagery, combined with support vector machine decoding to identify regions that contained shared neural representations across the presence and absence of visual input. Critically, we applied representational similarity analysis using a multimodal deep neural network (DNN) model comprising text and image encoders to dissociate language-structured and visual-structured knowledge representations. Comparisons between visualizers and aphantasics allowed us to test the relevance of voluntary imagery experience to these representations. We found that while both the ventral and dorsal pathways contained shared representations across conditions with and without visual presentation of meaningful objects, anatomically distinct regions supported different representational structures with varying links to imagery experience: (1) the left lateral occipitotemporal cortex (LOTC) encoded visual-structured knowledge representations, linked to imagery experience; (2) the bilateral fusiform gyrus, left dorsal LOTC, and right inferior frontal gyrus encoded language-structured knowledge representations, unrelated to imagery experience; and (3) the left superior parietal lobule encoded prior-knowledge-absent visual maintenance representations that were also unrelated to imagery experience. Together, these findings suggest that shared neural representations between the presence and absence of sensory input arise from multiple, functionally and computationally distinct mechanisms, which vary in their reliance on prior knowledge and imagery experience.

Introduction

Visual perception, conceptual knowledge, and mental imagery are closely related but functionally distinct cognitive processes. Perception involves processing external sensory input (perceiving the image of a *cat*); conceptual knowledge supports abstract, conceptual understanding of that object even without sensory input (understanding what *cat* is); and imagery generates internal visual experiences (visualizing in mind a *cat*). Substantial evidence suggests that both conceptual knowledge and visual imagery are (partly) rooted in internal representations derived from the perceptual systems.

In studies on object knowledge retrieval, visual regions are activated when participants answer questions given object names or cues. For instance, understanding object names activate the ventral occipitotemporal cortex respecting object domain organization (Bi et al., 2016; Chao et al., 1999; Devlin et al., 2005; He et al., 2013; B. Z. Mahon et al., 2009; M. V. Peelen et al., 2013; van den Hurk et al., 2017), and retrieving object color or shape properties activate regions in the fusiform gyrus and lateral occipital cortex, overlapping with those perceiving color and shape (Bannert & Bartels, 2013; Conway & Tsao, 2009; Hsu et al., 2011; M. V. Peelen et al., 2014; Xu et al., 2023). Even early visual cortex has been implicated in semantic representations (Vetter et al., 2014, 2020).

Parallel findings have emerged from studies on visual imagery. Participants activate early visual cortex when maintaining or reconstructing visual stimuli in the absence of external input (Breedlove et al., 2020; Kosslyn et al., 1999, 2001; Pearson & Kosslyn, 2015). Even when there is no increase in mean activity strength, specific visual content—such as orientation gratings or object identity—can still be decoded from multivoxel patterns in early visual cortex (e.g., Dijkstra et al., 2017; Harrison & Tong, 2009; Lee et al., 2012). Beyond early visual cortex, imagery-related representations have also been observed in higher-level regions including the fusiform gyrus (Spagna et al., 2021), lateral occipital cortex (Bannert & Bartels, 2018; Lee et al., 2012), and parietal cortex (Li et al., 2023; Xu & Chun, 2006).

These findings together suggest a potentially shared representations among object perception, knowledge, and imagery. This joint convergence raises a critical question: do imagery and knowledge retrieval rely on the same neural code, differing only in conscious access requirement (see discussions in Barsalou, 1999; Barsalou et al., 2003; Martin, 2007), or do they engage distinct representations at overlapping regions? Are these representations “visual”-related in nature by the virtual of overlapping with visual perception, i.e., aligning with the commonly held “embodied” (or “grounded”) notion (see reviews in Barsalou, 1999; Martin, 2016)?

Some evidence from congenital aphantasia (Zeman, 2024; Zeman et al., 2015)—a condition marked by a lifelong absence of visual imagery experience — has hinted that visual imagery and knowledge representation may have (at least partly) different neural substrates. Individuals with aphantasia exhibit preserved semantic knowledge despite lacking conscious imagery (J. Liu & Bartolomeo, 2023). Recent fMRI studies reveal that aphantasics retain latent early visual cortex representations to support decoding for natural sounds during passive tasks (e.g., listening to dog barking vs. traffic noise) but not during active (attempted) imagery generation for these sounds (Cabbai et al., 2024; Montabes de la Cruz et al., 2024). Furthermore, in a region of the left fusiform gyrus thought to be involved in imagery, the neural representational space of (attempted) object imagery in aphantasics, while resembling that of

visualizers, is less similar to perception than that of visualizers (J. Liu et al., 2025). That is, the neural representations during perception, imagery generation, and knowledge access may not be identical.

To understand the relationship between perception, imagery, and knowledge retrieval, we need to be more specific about the types of potential representations that may underlie the observed activation overlap or cross-task decoding success, and test them accordingly. We articulate the following possible types of internal object representations when visual stimuli are absent: 1) **a visual-experience-structured object knowledge representation** (**visual-knowledge** for short), i.e., object neural representations derived from past visual experiences; 2) a **language-experience-structured (nonvisual semantic) object knowledge representation** (**language-knowledge** for short), i.e., object representations derived from language experience; 3) a **visual maintenance representation not necessarily dependent on prior knowledge** (**priorless visual** for short) – when a visual stimulus is presented (with or without associated internal knowledge), there may be a period of maintenance in memory after it disappears. Note that the first two types of representations have been proposed based on behavioral and neural evidence (Bi, 2021; Paivio, 1991). While visual-knowledge representations are commonly assumed to reside in the visual cortex—given the observed overlap with perception (see above)—there is no evidence against the co-existence of nonvisual semantic object representations, especially considering that language and visual systems intrinsically interact (see discussions in Chen et al., 2025; Liu et al., 2025; Wang et al., 2020). Notably, congenitally blind people lack effects in visual cortex when retrieving pure visual properties (e.g., color; Wang et al., 2020) due to the complete absence of visual input, whereas congenitally aphantasic individuals have normal vision but are only 'blind' in mind. Orthogonal to the three representational types is the dimension of **conscious access**—any of these representations may or may not associate with imagery experience. Thus, six representational candidates are postulated in total (see Fig. 1 for this two-dimensional hypothesis space varying along representational structure and voluntary imagery relevance). These representational structures tend to correlate – for example, *cats* are more similar to *dogs* than to *tables* across all of them – and thus, cross-task decoding may be supported by any one or even multiple of these representations.

Here we carefully leverage the state-of-the-art large computation models, combined with populations with different imagery experience (visualizers vs. aphantasics), to examine these candidate internal neural representations. Specifically, we adopted CLIP (Contrastive Language-Image Pretraining) — a multimodal neural network trained on paired images and captions (Radford et al., 2021). CLIP comprises two parallel encoders: an image-encoder that captures visual similarity, and a text-encoder that captures semantic similarity. By correlating brain activity patterns with the representational structures derived from each encoder, we infer whether neural representations are more aligned with vision-derived-structure or language-derived-structure. We adopted CLIP for the main analyses because the paired training architecture and training datasets make the comparisons between vision and language easier.

Building on prior findings, we conducted fMRI experiments using a retro-cue paradigm (Dijkstra et al., 2017; Harrison & Tong, 2009) in both visualizers and aphantasics, with the following predictions along the two representation dimensions. Regarding information content, ***1) visual-knowledge representation***: If visual-experience-structured object knowledge supports shared representations, neural patterns should align with CLIP image-encoder in both perception and imagery; ***2) language-***

knowledge representation: If language-experience-structured object knowledge underlies shared representations, neural patterns should align with CLIP text-encoder in both perception and imagery; ***3) priorless visual representation***: If low-level visual maintenance is sufficient to support shared representations, then even meaningless shapes—lacking semantic associations—should be decoded above chance across perception and imagery. Regarding ***imagery experience*** relevance, we asked whether voluntary imagery is associated with these particular neural representations. If so, we should observe group differences between visualizers and aphantasics. If not, shared representations and specific representational structure should emerge in both groups. Together, this framework allowed us to probe both the structural format (visual vs. language) and cognitive basis (imagery-relevant vs. irrelevant) of shared neural representations that bridge the presence and absence of sensory input.

Methods

Participants

Seventeen healthy individuals with congenital aphantasia (mean age ± SD: 23 ± 3 years; 14 females) and twenty-two control participants with typical visual imagery (22 ± 2 years; 17 females) took part in the study. Aphantasia was identified using the Vividness of Visual Imagery Questionnaire (VVIQ, Marks, 1973), with scores below 32. Follow-up interviews ensured participants fully understood the instructions and confirmed the absence or near absence of visual imagery experience. All participants had normal or corrected-to-normal vision and hearing, and no history of psychiatric or neurological disorders. Informed consent was obtained from all participants, who received monetary compensation. The study was approved by the Institutional Review Board of the State Key Laboratory of Cognitive Neuroscience and Learning at Beijing Normal University, and adhered to the Declaration of Helsinki.

Stimuli

Three categories of images were used (Supplementary Fig. 1): two meaningful domains—animals (e.g., cat, tortoise, elephant, crab, panda, bee) and large objects (e.g., tea table, dressing table, bathtub, fence, sailboat, children's slide)—and one meaningless shape class. Meaningless shapes were drawn arbitrarily in Photoshop, filled with 10 × 10 pixel patches randomly sampled from the meaningful images, followed by 2D Gaussian blurring in MATLAB R2020a (v.2020a, MathWorks).

All images were converted to grayscale and normalized for luminance and contrast using the SHINE toolbox (Willenbockel et al., 2010). Familiarity and pixel-based inter-image dissimilarity between animal and large object images were matched (two-sample t-test ps > .08), as were those between meaningless and real objects ($p = .36$). The test images (used in the test phase; see Procedure) were visually similar but distinct exemplars and were excluded from further analyses.

Procedure

We employed a retro-cue paradigm (Dijkstra et al., 2017; Harrison & Tong, 2009; Fig. 2a). In each trial, two images were shown sequentially for 1 s each (perception phase), separated by a jittered interstimulus interval of 2 - 4 s. A numeric cue ('1' or '2') then indicated which image participants should

visualize during a subsequent 4 s blank interval (imagery phase). Finally, a test image was presented (test phase), and participants judged whether it was exactly the same image, not just the same object, as the cued one. Responses were made with the index fingers (left = "yes", right = "no"). Each trial lasted 17 s.

To optimize the experimental design, trial sequences were counterbalanced: the two sequentially presented stimuli always came from different categories, each had an equal probability of appearing first or second, and each was equally likely to be cued. Image pairings were unique across every four runs. The numbers of “yes” and “no” trials were also balanced. Each run contained 18 trials, such that within each run every item was imagined once and perceived twice.

Thirty-seven participants completed all 8 runs; two (one from each group) completed only 4 runs due to personal reasons.

Image acquisition

MRI data were collected on a Siemens Prisma 3T scanner using a 64-channel phased-array head coil at Beijing Normal University Neuroimaging Center. Functional images were acquired with a multi-band echo-planar imaging sequence: 64 axial slices, 2 mm thickness, phase encoding direction from posterior to anterior; 0.2 mm gap; multi-band factor = 2; TR = 2000 ms; TE = 30 ms; flip angle = 90°; matrix size = 104 × 104; FoV = 208*208; voxel size = 2 × 2 × 2 mm^3. Each task run lasted 5 minutes and 34 seconds (167 volumes). High-resolution T1-weighted anatomical images were collected with a 3D MPRAGE sequence: 192 sagittal slices; 1 mm thickness; TR = 2530 ms; TE = 2.98 ms; TI = 1100 ms; flip angle = 7°; FoV = 224 × 256 mm^2; voxel size = 0.5 × 0.5 × 1 mm^3, interpolated; matrix size = 224 × 256.

Data preprocessing

Functional data preprocessing was conducted in SPM12 (SPM12 Software - Statistical Parametric Mapping) using MATLAB R2020a (v.2020a, MathWorks). The first 6 volumes, acquired during the initial fixation period, were discarded. The remaining data underwent slice-timing correction, motion correction, and high-pass filtering (cutoff: 0.008 Hz). Data were normalized to Montreal Neurological Institute (MNI) space using unified segmentation and resampled to 2 mm isotropic voxels

Data analysis

Behavioral Performance. For each participant and stimulus class, we computed accuracy and performed a repeated-measures ANOVA with group and stimulus class as factors. For reaction times (RT), we included only correct trials and excluded outliers beyond ±3 standard deviations. RTs were then averaged across trials for each participant and class, followed by another repeated-measures ANOVA with the same factors.

GLM Construction. We modeled each subject’s data using a general linear model (GLM) for each run in SPM12. Predictors of interest included all items during perception, imagery, and test, with six motion parameters included as nuisance regressors. All predictors were convolved with the canonical hemodynamic response function. Since the test phase was only used to ensure task engagement, corresponding data were excluded from further analyses. For multivariate decoding analyses, beta

images were spatially smoothed using a 2-mm FWHM Gaussian kernel (Hendriks et al., 2017; Op de Beeck, 2010).

Searchlight SVM Decoding Analysis. Searchlight analysis was restricted to a whole-brain gray matter mask, defined as voxels with probability > 1/3 in the SPM12 gray matter template and located within cerebral regions (1 - 90) of the Automated Anatomical Labeling (AAL) atlas, yielding 122,694 voxels (981,552 mm^3). For each voxel, we defined an 8-mm radius sphere (257 voxels) and extracted beta estimates for each item and run, normalized within the sphere. We employed repeated split-half cross-validation(Valente et al., 2021), exhaustively iterating through all possible data splits, yielding 70 combinations for participants with 8 runs and 6 combinations for those with 4 runs. In each split, perception data from one half were used to train an SVM classifier, which was then tested on imagery data from the other half—and vice versa (Fig. 2a). The mean accuracy across both directions and all splits was assigned to the sphere's center voxel. Group-level statistical inference was performed using permutation-based Statistical nonParametric Mapping (SnPM) (NISOx: SnPM), with 5000 permutations and no variance smoothing. Cluster-level FWE correction was applied for multiple comparisons, as it is the only method implemented in the software for cluster-level inference. All searchlight decoding results were thresholded at voxelwise $p < .001$, cluster-level FWE-corrected $p < .05$, unless stated otherwise. Domain-level decoding classified animals vs. large objects; item-level decoding classified among individual object identities.

Searchlight CLIP Model RSA. CLIP is a neural network trained on a variety of image-text pairs, being adapted by the alignment between images and their corresponding text descriptions (Radford et al., 2021). We utilized a Chinese version of CLIP (Yang et al., 2023), pretrained on around 200 million publicly available image-text pairs data in Chinese, using the ViT-L/14 architecture for the image-encoder and RoBERTa-wwm-Base for the text-encoder. We extracted embeddings for each image and its label (e.g., "cat," "elephant," "dressing table" in Chinese) from the penultimate layers of the encoders (i.e., 23rd out of 24 layers for the image-encoder, and 11th layer for the text-encoder), and computed representational dissimilarity matrices (RDMs) based on cosine distance, yielding image-RDM and text-RDM, respectively. We used embeddings from the penultimate layer rather than the output layer (as in Chen et al., 2025; Shoham et al., 2024), because they preserve rich modality-specific representational structure while avoiding potential distortions from the final alignment step optimized for contrastive learning.

Searchlight RSA was conducted within the cross-decoding mask (Fig. 2c-ii), defined by a one-sample t-test across all subjects (voxelwise $p < .001$, cluster-level FWE-corrected $p < .05$). Neural RDMs were computed for each subject by extracting T-value vectors from searchlight spheres (as in the decoding analysis), and measuring dissimilarities as 1 − Pearson correlation between stimulus pairs. We then computed Spearman partial correlations between neural RDMs and one encoder RDM, controlling for the other, and used commonality analysis (Nalborczyk, 2025) to quantify shared variance among all three RDMs. Coefficients were assigned to the center voxel of each sphere. Group-level analyses were also performed using permutation-based Statistical nonParametric Mapping (SnPM) (NISOx: SnPM), with 5000 permutations and no variance smoothing. Results were thresholded at voxelwise $p < .001$, cluster-level FWE-corrected $p < .05$, unless stated otherwise.

ROI-based RSA with CLIP Model Layers. To explore whether the encoders' effects differ in different processing stages in the two groups, we conducted ROI-based RSA across multiple stages of the encoders. We extract layerwise features from the Chinese-CLIP model by registering forward hooks on each residual block of the visual transformer and each encoder layer of the BERT-based text encoder. During a forward pass, we collected the [CLS] token embeddings from each layer for both image and text inputs. For image processing, preprocessed images were passed through the visual encoder, and for text, tokenized captions were passed through the text encoder. At each layer, [CLS] embeddings were detached, stored, and stacked across stimuli. Cosine similarity matrices were computed from L2-normalized features, and converted into RDMs by subtracting similarity from one. Correlations and partial correlations between neural RDMs and encoder RDMs were computed within the defined ROIs (see Results). For partial correlations, the penultimate layer RDM of the non-target encoder was regressed out. We grouped the layers into three equal parts as early, middle, and late layers, averaged layer values within each layer-group for each subject, and performed statistical analyses at the layer-group level. We also conducted agglomerative clustering for the RDMs derived from the layers of each encoder to group them into different processing stages to repeat this analysis (see Supplementary Fig. 8-9). All correlation coefficients were Fisher-Z transformed prior to statistical analysis in R.

All statistical analyses of behavioral and ROI data were conducted in R (R Core Team, 2019) using the rstatix package (Kassambara, 2021). Two-sample comparisons were performed with Welch's t-test, which adjusts for unequal sample sizes(Delacre et al., 2017).

Results

To explore the representational mechanisms underlying seemingly shared neural patterns across the presence and absence of visual input, and to examine their relevance to voluntary imagery, we conducted an fMRI experiment using a retro-cue visual working memory paradigm (Fig. 2a) in individuals with (visualizers) and without (aphantasics) visual imagery. We first analyzed behavioral performance to ensure that both groups performed the task well. Next, we conducted searchlight SVM cross-decoding to identify brain regions supporting (at least some) shared representations across perception and imagery phases for both meaningless and real objects. Within the regions identified for real objects (i.e., with internal knowledge representations), we applied searchlight RSA using a Chinese CLIP model to dissociate visual- vs. language-derived representational structures, and to examine their relevance for conscious imagery experience by comparing visualizers and aphantasics. Finally, layer-wise ROI-based RSA was conducted to explore the neural representational similarity profiles across different processing hierarchies of the encoders.

Behavioral results

To test whether aphantasics could perform the retro-cue working memory task as well as visualizers, we analyzed participants' behavioral performance in the scanner. As shown in Fig. 2b, repeated-measures ANOVA on accuracy revealed no significant main effect of group ($F_{(1, 37)} = 1.17$, $p = .29$, $\eta^2 = .03$), stimulus class ($F_{(2, 74)} = 0.99$, $p = .38$, $\eta^2 = .005$), or their interaction ($F_{(2, 74)} = 0.78$, $p = .46$, $\eta^2 = .004$).

For reaction time (RT), repeated-measures ANOVA showed no significant main effect of group ($F_{(1, 37)} = 0.05$, $p = .82$, $\eta^2 = .001$) or interaction ($F_{(2, 74)} = 2.96$, $p = .06$, $\eta^2 = .001$), but a significant main effect of

stimulus class ($F_{(2, 74)} = 6.01$, $p = .004$, $\eta^2 = .002$). Pairwise comparisons indicated that responses to meaningless shapes were significantly slower than responses to animals or large objects (ps < .02, FDR-corrected). That is, performance differences were driven by stimulus properties rather than group, indicating that aphantasic participants performed the task as accurately and efficiently as visualizers.

Searchlight SVM decoding results: Shared neural representations across perception-imagery phases identified

To identify brain regions supporting (some) shared neural representations between perception and imagery phases, we conducted whole-brain searchlight SVM cross-decoding analyses for meaningless shapes and real objects, respectively. A repeated split-half cross-validation approach was used, where an SVM classifier was trained on perception data from half of the runs and tested on imagery data from the remaining half, and vice versa. This procedure was repeated across a grey matter mask. For each searchlight sphere, the decoding accuracy was averaged across all split-half combinations and both train-test directions, and the resulting value was assigned to the center voxel. Group-level statistical inference was conducted using permutation test. Results were thresholded at voxelwise $p < .001$, cluster-level FWE-corrected $p < .05$, unless stated otherwise.

The left SPL contained shared representations across the perception and imagery phases for meaningless shapes (priorless visual representation) in both aphantasics and visualizers.

To assess whether visual maintenance alone is sufficient to support shared neural representations between the perception and imagery phases, we conducted searchlight SVM cross-decoding for meaningless shapes (6-way classification). We first pooled all subjects together to perform group-level inference to maximize sensitivity to identify the areas containing shared neural representations across the perception and imagery phases in all subjects. The result showed a significant cluster in the left superior parietal lobule (SPL; Fig. 2c-i; voxelwise $p < .005$, cluster-level FWE-corrected $p < .05$; not surviving multiple correction at voxelwise $p < .001$). Mean decoding accuracy extracted from this SPL cluster did not differ between groups ($t_{(36.9)} = 0.03$, $p = .97$), indicating that the perception-like representations for maintaining meaningless shapes were contained in the dorsal stream irrespectively of voluntary imagery.

When tested separately for each group, no significant above-chance decoding was found in either group after multiple comparisons correction. An uncorrected trend showed that the effects in visualizers distributed across both ventral and dorsal regions, whereas in aphantasics mainly in dorsal regions. Group comparison did not reveal statistically survived clusters (see Supplementary Fig. 2 for the uncorrected maps).

The VOTC areas contained shared representations across the perception and imagery phases for real objects (Knowledge-Scaffolded representation) in both aphantasics and visualizers.

For real objects with prior knowledge, we examined brain regions that contained common representations of domains (animal vs. large object) across the perception and imagery phases. As shown in Fig. 2c-ii, the result of group-level analysis combining all subjects revealed significant cross-decoding in the bilateral ventral occipitotemporal cortex (VOTC), with extensions into the left lateral

occipital cortex (LOC), as well as in the right inferior frontal gyrus (IFG). Mean decoding accuracy extracted from these regions did not differ between groups ($t_{(27.9)} = -0.29$, $p = .77$).

The group-level result of each group (Supplementary Fig. 3) showed that visualizers had successful cross-decoding for domains in bilateral VOTC, extending to the left LOC. By contrast, the aphantasic group showed significant decoding only in the right fusiform gyrus (FG). All these areas were included in the regions identified by the combined group-level result. We then tested group differences by voxels within these regions. The result showed a trend toward higher accuracy in the left ventral lateral occipitotemporal cortex (LOTC) in the visualizers; however, it could not survive multiple comparisons correction (see Supplementary Fig. 3 for an uncorrected result).

We further conducted an item-level cross-decoding (12-way classification) for real objects. This analysis revealed similar but spatially more restricted results (Supplementary Fig. 4) than domain-level decoding. Pooled group-level result showed a distribution across VOTC that largely overlapped with the domain-level decoding result. The visualizer group showed significant decoding in the left FG, and the aphantasic group showed significant decoding in the right lateral FG. However, no significant group differences were observed, even under a liberal uncorrected threshold of $p < .01$.

These results suggest that the VOTC regions contained shared representations across the perception and imagery phases in both groups, with only a trend of effect of imagery experience in the left ventral LOTC. Given that successful cross-decoding alone does not reveal what types of underlying representational structures support such decoding, we performed searchlight RSA to dissociate representational structures within the combined group-level domain cross-decoding mask (i.e., the regions shown in Fig. 2c-ii)

Searchlight CLIP-model-based RSA results: Multiple representation types identified

To dissociate these representational structures, we leveraged a Chinese version of the multimodal deep neural network CLIP (Radford et al., 2021; Yang et al., 2023), which consists of an image-encoder and a text-encoder aligned in a shared embedding space. We employed searchlight RSA in the cross-decoding mask (Fig. 2c-ii) to examine the similarity between neural representations (during perception phase and during imagery phase) and the representational structures of each encoder. We input the stimuli images into the image-encoder and the names of the objects into the text-encoder, extracted the features from the *penultimate layers*, and transformed them into RDMs based on cosine distance (Fig. 3a). There was a medium-level, significant correlation between the RDMs of the two encoders ($r = 0.40$, $p < .001$). Therefore, we partitioned the variance into components specific to each model, as well as the shared variance contributing to the explanation of the neural RDMs, using partial correlations and commonality analysis (Nalborczyk, 2025). Because the shared variance among image-, text-, and neural-RDMs cannot be unambiguously assigned to either representational structure, we focused on the unique contributions of the image- and text-encoders to the neural representations.

Both unique language- and visual-knowledge representations existed in visualizers.

In visualizers (Fig. 3b, top), during the perception phase, partial correlations between neural and CLIP text-encoder RDMs (blue) appeared in the bilateral FG, left dorsal LOTC, and right LOTC. During the imagery phase, effects were restricted to the left FG and left dorsal LOTC.

Partial correlations with the CLIP image-encoder RDM (orange-red) during the perception phase were distributed across the bilateral FG and extended into the bilateral LOTC. No significant effects emerged during the imagery phase (see the map covered by the grey box in Fig. 3b and Supplementary Fig. 5 for uncorrected results).

Commonality analysis (green) revealed shared variance among neural, image-encoder, and text-encoder RDMs in the bilateral FG during the perception phase, with no significant clusters during the imagery phase even at the highly lenient threshold of $p < .05$.

Only unique language-structured representations existed in aphantasics.

In the aphantasic group (Fig. 3b, bottom), partial correlations with the CLIP text-encoder RDM were observed during the perception phase in the bilateral FG, left dorsal LOTC, and right LOTC, consistent with the visualizer group. During the imagery phase, only a cluster in the right lateral FG was observed. No significant correlations with the CLIP image-encoder RDM were observed during either the perception or imagery phase. Commonality effects were observed in the right FG during the perception phase but not observed during the imagery phase (see maps covered by the grey boxes in Fig. 3b and Supplementary Fig. 5 for uncorrected results).

Group difference existed in visual-structured representations during the perception phase.

Two-sample t-tests within the mask (Fig. 3b, right) revealed significant group differences specifically for the effect of CLIP image-encoder RDM, with visualizers showing greater model-neural similarity than aphantasics in the left LOTC. No significant group differences emerged in similarity to the CLIP text-encoder RDM, either during the perception phase or the imagery phase (see Supplementary Fig. 6 for uncorrected results).

Summary

To summarize the searchlight CLIP RSA findings, two types of representations with different relevance to voluntary imagery experience emerged:

One type was observed in both groups, showing reliable similarity to the CLIP text-encoder (penultimate layer representations) during both the perception and imagery phases, without significant group differences. We therefore combined all subjects (visualizers and aphantasics) to perform group-level inference, enhancing the common effect of the CLIP text-encoder, and overlaid the statistical maps from the perception and imagery phases (Fig. 4, blue areas; Supplementary Fig. 7). Overlapping regions were observed in the bilateral FG, left dorsal LOTC, and right IFG. These regions likely represent objects in terms of their relations within the language space, supporting both perception and imagery, and their involvement does not depend on voluntary imagery experience. That is, having representations here does not determine whether one can mentally visualize objects. We refer to these regions as **"Language-knowledge-imagery-irrelevant."**

Another type was observed only in the visualizer group, showing significant similarity to the CLIP image-encoder (penultimate layer representations) during the perception phase, with a significant group difference in the left LOTC (Fig. 4, orange area). This region likely represents objects in terms of their visual experiential properties in typical populations, and the absence of such representations is associated with the lack of voluntary visual imagery. We refer to this region as **"Visual-knowledge-imagery-relevant".**

ROI-based RSA results: In-depth-analyses with different model hierarchies

In this section we zoom into the two types of regions of interest (ROIs) identified above -- "Language-knowledge-imagery-irrelevant" ROIs, including the left dorsal LOTC, bilateral FG, and right IFG (blue areas in Fig. 4); "Visual- knowledge-imagery-relevant" ROI, i.e., the left LOTC (orange area in Fig. 4) -- to characterize their representational profiles, referencing to representations at different layers of the target DNN models.

Visualizers and aphantasics converged across multiple stages in similarity to the CLIP-text-encoder.

To test whether representational similarity to the text-encoder differed between groups at earlier representational hierarchies, we grouped the text-encoder layers into three parts: early (layers 1 - 4), middle (5 - 8), and late (9 - 12) (see layerwise results in Supplementary Fig. 8). Features from all layers were extracted and converted into RDMs, which were then used to compute correlations and partial correlations with neural RDMs of the language-knowledge-imagery-irrelevant ROIs (i.e., left dorsal LOTC, bilateral FG, and right IFG). As regressing out a specific RDM (i.e., the penultimate layer RDM of the non-target encoder) was not fair for all layers of the target encoder, statistical inferences were performed directly on the mean Fisher-Z-transformed correlations, instead of partial correlations, of the layer-groups. As shown in Fig. 4a, both visualizers and aphantasics exhibited an increasing trend in similarity from early to late layers in all ROIs during both the perception and imagery phases.

During the perception phase, a mixed ANOVA with factors subject-group (visualizers, aphantasics), layer-group (early, middle, late), and ROI revealed a significant main effect of layer-group ($F_{(2,74)} = 23.41$, $p = 1.32 \times 10^{-8}$, $\eta^2 = 0.08$) and a significant interaction between layer-group and ROI ($F_{(6,222)} = 2.3$, $p = 0.04$, $\eta^2 = 0.02$). Simple effects test indicated significant layer-group effect in the left FG and left MTG (Fs > 6.33, ps < .004, FDR-corrected), with the late layers being significantly higher than the former two layer-groups (ps < 0.01, FDR-corrected) but no difference between the early and middle layers (ps > 0.22, FDR-corrected). The right FG and right IFG showed marginally significant simple effects of layer-group (Fs < 2.57, ps > 0.08, FDR-corrected), with only a trend of significant difference between the late and early layers (ps > .07, FDR-corrected). No effects of subject-group, ROI, or their interactions were observed (Fs < 1.11, ps > .36).

During the imagery phase, the mixed ANOVA revealed a significant main effect of layer-group ($F_{(2,74)} = 11.58$, $p = 4.21 \times 10^{-5}$, $\eta^2 = 0.05$). Pairwise comparisons showed late > middle and late > early (ps < .004, FDR-corrected), with no early-middle difference (p = .13, FDR-corrected). No effects of group, ROI, or interactions were observed (Fs < 1.45, ps > .23).

We also grouped layers by clustering for the RDMs derived from all layers (Supplementary Fig. 8). Results were consistent with the main analyses. During the perception phase, there was a main effect of layer-group ($F_{(2,74)} = 17.83$, $p = 4.77 \times 10^{-7}$, $\eta^2 = 0.08$), with late > middle and early (ps < 3.44×10^{-5}, FDR-corrected), and early not differing with middle (p = .09, FDR-corrected). During the imagery phase, a main effect of layer-group was also observed ($F_{(2,74)} = 11.49$, $p = 4.5 \times 10^{-5}$, $\eta^2 = 0.06$), with late and middle > early (ps < 1.69×10^{-4}, FDR-corrected), but no significant difference between late and middle (p = .35, FDR-corrected).

Together, these findings validate that language-knowledge-imagery-irrelevant representations (i.e., left dorsal LOTC, bilateral FG, and right IFG) in visualizers and aphantasics converged across multiple layers, with representational similarity to the text-encoder increasing at later, more abstract layers.

Visualizers and aphantasics differed at later layers in similarity to the imagery-encoder, during both the perception and imagery phases.

For RSA in the visual-knowledge-imagery-relevant ROI (i.e., left LOTC), we also grouped the layers of the image-encoder into three parts: early (layers 1 - 8), middle (9 - 16), and late (17 - 24) (see the layerwise result in Supplementary Fig. 9). As shown in Fig. 4b, during the perception phase, similarity to the image-encoder was significantly above zero in both visualizers and aphantasics at the early and middle layers (ts > 2.73, ps < .02, FDR-corrected) but diverged at the late layers. A mixed ANOVA with factors subject-group (visualizers, aphantasics) and layer-group (early, middle, late) revealed a significant interaction effect ($F_{(2,74)} = 15.39$, $p = 2.58 \times 10^{-6}$, $\eta^2 = 0.08$). Simple effects showed a significant subject-group difference at the late layers ($t_{(34.5)} = 4.75$, $p = 3.46 \times 10^{-5}$, FDR-corrected), but not at the early or middle layers (ts < 0.83, ps > 0.62, FDR-corrected).

During the imagery phase, similarities to the image-encoder were significant in visualizers across all layer-groups (ts > 2.27, ps < .04, FDR-corrected) but not in aphantasics (ts < 1.11, ps > .21, FDR-corrected). However, no main effects of subject-group or subject-group × layer-group interactions were observed (Fs < 1.56, ps > .22). We then took another approach to test the effect of imagery experience on the neural representational similarity to the image-encoder by calculating correlations between the mean similarity values (i.e., the correlation between the neural RDM and image-encoder RDM) and VVIQ scores across individuals. Mean similarity at the late layers significantly correlated with VVIQ scores across all subjects (Spearman's $\rho = 0.39$, p = .04, FDR-corrected; Fig. 4b, right), but not at the early or middle layers (Spearman's ρs < 0.28, ps > 0.08, FDR-corrected). Within-subject-group analysis revealed a significant correlation between the similarity to the image-encoder and VVIQ scores in visualizers (Spearman's $\rho = 0.51$, p = .03, FDR-corrected) but not in aphantasics (Spearman's $\rho = 0.22$, p = .39, FDR-corrected).

We also tested whether similarity to the image-encoder correlated with VVIQ scores in visualizers during the perception phase, but no association was found (Spearman's $\rho = 0.11$, p = .61, uncorrected), indicating that subjective imagery vividness does not tract the visual-structured representation during object perception, and instead is a property for the imagery process.

An alternative layer-group partitioning approach based on clustering (Supplementary Fig. 9) yielded consistent results. During the perception phase, a mixed ANOVA revealed a significant subject-group ×

layer-group interaction ($F_{(2,74)} = 14.72$, $p = 3.89 \times 10^{-8}$, $\eta^2 = 0.09$), with significant subject-group differences at the mid-late and late layers (ts > 3.70, ps < .002, FDR-corrected). During the imagery phase, no significant effects were observed in the mixed ANOVA. Correlation analysis showed that similarity to the image-encoder correlated with VVIQ scores across all subjects at the mid-late and late layers (Spearman's ρs > 0.36, ps < .05, FDR-corrected), with a significant correlation in visualizers at the mid-late layers (Spearman's $\rho = 0.49$, $p = 0.04$, FDR-corrected).

Although no significant clusters were observed in the searchlight analysis with the penultimate layer in visualizers during the imagery phase (Fig. 3b, top), the late layers overall showed significant similarity to the image-encoder in the ROI analysis. Inspection of the layerwise correlation profile (Supplementary Fig. 9) revealed a drop in correlation at the last two layers. To examine whether other areas contained image-encoder-like representations during the imagery phase, we selected layer 18—the later layer with the highest average correlation across all subjects in the ROI analysis—and used its RDM for whole-brain searchlight RSA. This analysis (Supplementary Fig. 10) revealed significant clusters in the bilateral ventral LOTC and left LOC, again with a significant group difference in the left ventral LOTC (Visualizers > Aphantasics). Importantly, the cluster location in the left LOTC could not be attributed to the choice of the optimal layer within the ROI of left LOTC, as a trend of such group difference was already present in this area in the searchlight RSA with the penultimate layer (Supplementary Fig. 6).

These results further elucidate that the visual-structured representation observed in the visual-knowledge-imagery-relevant ROI is related to conscious imagery experience particularly at later vision model layers, during both the perception and imagery phases.

Discussion

We investigated how conceptual knowledge representation and mental imagery relate to the shared neural representations across the presence and absence stage of visual input (as defined by areas supporting cross-process decoding). Specifically, what are the relationships among neural representations for seeing a *cat*, imagining a *cat*, and the internal memory storage of *cat*? Using a retro-cue fMRI paradigm separating the seeing phase and maintaining phase, we leveraged language- and vision-DNNs to test the object neural knowledge representation content (language-structured vs. visual-structured), and the contrast between individuals with and without visual imagery to test their relevance to conscious imagery experience (imagery-relevant vs. imagery-irrelevant).

We identified three types of neural representations that are common between visual-present and -absent phases (Fig. 5): 1) One type of object neural representation that is specifically fitted by vision model, is present in visualizers (as a function of subjective imagery vividness during imagery) but absent in aphantasics, i.e., a **visual-knowledge-imagery-relevant representation**, and is localized to the left LOTC; 2) Another type of object neural representation that is specifically fitted by language model, is present in both visualizers and aphantasics, i.e., a **language-knowledge-imagery-irrelevant representation**, and is localized to the left dorsal LOTC, bilateral FG, and right IFG; 3) A final type supporting novel meaningless shapes decoding in both visualizers and aphantasics, i.e., a **priorless-imagery-irrelevant visual representation**, and is localized to the left SPL**.**

Multifaceted object knowledge representations

The nature of object representation in the ventral visual cortex is one of the classical topics in cognitive neuroscience, and has been difficult to reconcile (see reviews in Martin, 2016). Overlap between knowledge retrieval and perception, along with parsimonious principle, has led to the default assumption that it is visual and/or multimodal computations that converge with shape or other geometrical properties that vary by object domains/categories (see discussions in Martin, 2016; and about results with congenitally blind individuals in Bi et al., 2016). Here we showed two further dimensions of heterogeneity – object content organization more fitted with vision or language, and the involvement in subjective imagery experience. Specifically, the FG showed strong similarity with CLIP text-encoder, consistent with its role in multimodal and abstract object representations (Bi et al., 2016; Caramazza & Mahon, 2003; Mahon & Caramazza, 2011), irrelevant to imagery experience. The LOTC showed subregional characteristics: while it aligned with the image-encoder and tracked imagery vividness, suggesting a visual-structured, imagery-relevant format, the left dorsal subregion additionally aligned with the text-encoder, indicating a language-structured content. These results enrich our understanding of LOTC as a heterogeneous convergence zone, where representations of varied content reside (e.g., tool objects, action, shape knowledge; Chao et al., 1999; Martin et al., 1996; Wurm & Caramazza, 2019, 2022; Xu et al., 2023), suggesting that future studies on LOTC should consider the role of imagery processes and representational structures.

The right IFG is not typically discussed relating to conceptual knowledge but is frequently implicated in tasks requiring auditory working memory (e.g., maintaining tones or semantic information; Koelsch et al., 2009; Kumar et al., 2016; Schneiders et al., 2012; Shivde & Thompson-Schill, 2004; Uluç et al., 2018), and is also considered a critical region for cognitive inhibitory control (Aron et al., 2004, 2014). In the retro-cue task of the current experiment, although participants may have needed to suppress non-target stimuli during the imagery phase after the cue, inhibitory control alone cannot account for the significant cross-decoding observed for the target stimulus. Instead, our finding that the right IFG encoded language-structured object representations aligns more closely with prior auditory working memory studies, suggesting that internal representations do not necessarily mirror the modality of external input when maintaining information.

It is important to note that better fitting with CLIP text-encoder (and other large language models) by itself does not necessarily imply that the neural representation is processing language by nature. It is possibly still representing nonlinguistic aspects of objects that reflect relations that are better captured by language-derived higher-level semantics (see similar discussions in Chen et al., 2025; Conwell et al., 2025; Wang et al., 2023). Here the results simply suggest that the neural structures for objects are better explained by specific relational structures parallel those derived from language than from vision, and this type of representation is similarly present for visualizers and aphantasics, irrelevant to subjective imagery experience.

Functional localization of object imagery experience

Theoretical models of mental imagery propose a top-down reconstruction process, such that higher-level stored content is transformed into visual detail in lower-level sensory cortices (see reviews in Pearson, 2019, 2020). However, the timing and location of this reconstruction remain unclear. Our results show that while object knowledge is broadly represented in regions supporting shared perception-imagery patterns, imagery-specific content was confined to the left LOTC. How well the neural representation here during imagery fits with the CLIP image-decoder is predictive of how vivid an individual experiences subjective imagery. This region is close to the so-called fusiform imagery node (FIN) proposed to support domain-general internal visualization (Spagna et al., 2021, 2024). Prior work has shown reduced imagery-perception similarity, measured by the correlation between objects imagery-RDM and perception-RDM, in aphantasics, and positive associations with imagery vividness in visualizers in this node(J. Liu et al., 2025). Our findings support the critical role of this area in imagery function, and further revealed that in aphantasics not only the neural representations for imagery, but also those underlying perception, are altered to less "visual"-like (see discussion in the next section). However, this imagery effect may be limited to object-level stimuli. Earlier studies using low-level visual features (e.g., gratings, lines) have localized imagery effects to early visual cortices (Chang et al., 2025; Keogh et al., 2020), which were not observed in the current study using object-level materials, suggesting that the neural basis of imagery may vary by stimulus complexity—a question for future research.

For meaningless shapes that lack prior knowledge, left SPL emerged as the key site of shared representation between perception and imagery. This is consistent with its role in visual working memory (Koenigs et al., 2009; Li et al., 2023; Xu, 2018) and sub-conscious processing (Almeida et al., 2008; Fang & He, 2005; Maclean et al., 2023; Suzuki et al., 2014). In particular, aphantasics showed comparable SPL representations despite lacking subjective imagery, reinforcing the idea that consciousness-independent visual coding can be implemented via dorsal-stream mechanisms.

Diverse representations during perception

Intriguingly, in the aphantasic group, visual-structured representations of left LOTC at low to mid-levels were preserved during perception, but group differences emerged at higher layers. This implies that aphantasia may not only reflect a deficit in internal imagery, but a broader reorganization of perceptual encoding strategies. While visualizers and aphantasics perceived the same stimuli, their underlying neural organizations diverged.

However, we found no correlation between the vision-aligned representation during perception and VVIQ in visualizers, implying that this perceptual group difference is not directly modulated by conscious imagery vividness. Instead, it may reflect a compensatory shift toward language-based processing in aphantasics—a finding with implications for how we understand cognitive diversity in perception. Additionally, both visual-structured and language-structured representations—along with their shared variance—were significant in the ventral visual cortices in visualizers during perception, emphasizing the integration of both bottom-up and top-down (language-modulated knowledge structures) processes during perception.

The relationship between object perception, knowledge, and imagery experience

Although both object knowledge access and imagery generation engage the perceptual systems, our findings indicate that they rely on both shared and distinct representational mechanisms. Object

knowledge access and perception aligned in both the language-structured and visual-structured-representational space, while subjective imagery experience and perception aligned in the visual-structured space. These distinctions highlight that each process entails multiple types of representations, and the seemingly overlapping neural representations with a same process can arise from different types of representations. Note that for meaningless shapes without knowledge priors, while the left SPL was the strongest site of cross-decoding, we observed a trend the in ventral visual regions among visualizers. Whether the association between voluntary imagery experience and visual-structured representations in the left LOTC only applies to those with internal stores (memory), or can also arise from temporary bottom-up visual inputs, remains an open question for future studies to directly test.

Conclusion

Our findings reveal that shared neural representations across the presence and absence of sensory input arise from multiple, heterogeneous mechanisms: Visual-structured object knowledge representations emerged specifically in the left LOTC and were related to imagery experience. Language-structured knowledge representations were distributed in multiple areas across VOTC, invariant to imagery experience. Knowledge-absent and imagery-irrelevant visual representations were localized to the left SPL. Together, these results offer a more nuanced account of how object knowledge and mental imagery interact to support internal representations in human mind. They also underscore the value of integrating computational modeling, individual differences, and multivariate neuroimaging to uncover the representational architecture of the human brain.

Acknowledgement

We thank Jiahui Lu, Haojie Wen, and Ziyi Xiong for their assistance with data collection; Ze Fu for his advice on the analysis; Haoyang Chen for his assistance with the utility of the DNN models; Ze Fu, Haojie Wen, and Huichao Yang, for their advice on the figures; Yiyang Cai and Ziyi Xiong for their advice on the manuscript.

Funding

STI2030-Major Project 2021ZD0204100 (2021ZD0204104 to Y.B.); National Natural Science Foundation of China (31925020 and 82021004 to Y.B.); the Fundamental Research Funds for the Central Universities (Y.B.); China Postdoctoral Science Foundation funded project (2025M773448 to S.T.)

DNN models were acquired from: https://github.com/OFA-Sys/Chinese-CLIP

References

Almeida, J., Mahon, B. Z., Nakayama, K., & Caramazza, A. (2008). Unconscious processing dissociates along categorical lines. *Proceedings of the National Academy of Sciences*, *105*(39), 15214–15218. https://doi.org/10.1073/pnas.0805867105

Aron, A. R., Robbins, T. W., & Poldrack, R. A. (2004). Inhibition and the right inferior frontal cortex. In *Trends in Cognitive Sciences* (Vol. 8, Issue 4, pp. 170–177). https://doi.org/10.1016/j.tics.2004.02.010

Aron, A. R., Robbins, T. W., & Poldrack, R. A. (2014). Inhibition and the right inferior frontal cortex: one decade on. *Trends in Cognitive Sciences*, *18*(4), 177–185. https://doi.org/10.1016/j.tics.2013.12.003

Bannert, M. M., & Bartels, A. (2013). Decoding the yellow of a gray banana. *Current Biology*, *23*(22), 2268–2272. https://doi.org/10.1016/j.cub.2013.09.016

Bannert, M. M., & Bartels, A. (2018). Human V4 activity patterns predict behavioral performance in imagery of object color. *Journal of Neuroscience*, *38*(15), 3657–3668. https://doi.org/10.1523/JNEUROSCI.2307-17.2018

Barsalou, L. W. (1999). Perceptual symbol systems. *Behavioral and Brain Sciences*, *22*(4), 577–660. https://doi.org/10.1017/S0140525X99002149

Barsalou, L. W., Kyle Simmons, W., Barbey, A. K., & Wilson, C. D. (2003). Grounding conceptual knowledge in modality-specific systems. *Trends in Cognitive Sciences*, *7*(2), 84–91. https://doi.org/10.1016/S1364-6613(02)00029-3

Bi, Y. (2021). Dual coding of knowledge in the human brain. *Trends in Cognitive Sciences*, *25*(10), 883–895. https://doi.org/10.1016/j.tics.2021.07.006

Bi, Y., Wang, X., & Caramazza, A. (2016). Object Domain and Modality in the Ventral Visual Pathway. *Trends in Cognitive Sciences*, *20*(4), 282–290. https://doi.org/10.1016/j.tics.2016.02.002

Breedlove, J. L., St-Yves, G., Olman, C. A., & Naselaris, T. (2020). Generative Feedback Explains Distinct Brain Activity Codes for Seen and Mental Images. *Current Biology*, *30*(12), 2211-2224.e6. https://doi.org/10.1016/j.cub.2020.04.014

Cabbai, G., Racey, C., Simner, J., Dance, C., Ward, J., & Forster, S. (2024). Sensory representations in primary visual cortex are not sufficient for subjective imagery. *Current Biology*, *34*(21), 5073-5082.e5. https://doi.org/10.1016/j.cub.2024.09.062

Caramazza, A., & Mahon, B. Z. (2003). The organization of conceptual knowledge: The evidence from category-specific semantic deficits. *Trends in Cognitive Sciences*, *7*(8), 354–361. https://doi.org/10.1016/S1364-6613(03)00159-1

Chang, S., Zhang, X., Cao, Y., Pearson, J., & Meng, M. (2025). Imageless imagery in aphantasia revealed by early visual cortex decoding. *Current Biology*. https://doi.org/10.1016/j.cub.2024.12.012

Chao, L. L., Haxby, J. V., & Martin, A. (1999). Attribute-based neural substrates in temporal cortex for perceiving and knowing about objects. *Nature Neuroscience*, *2*(10), 913–919. https://doi.org/10.1038/13217

Chen, H., Liu, B., Wang, S., Wang, X., Han, W., Zhu, Y., Wang, X., & Bi, Y. (2025). *Language modulates vision: Evidence from neural networks and human brain-lesion models*. http://arxiv.org/abs/2501.13628

Conway, B. R., & Tsao, D. Y. (2009). Color-tuned neurons are spatially clustered according to color preference within alert macaque posterior inferior temporal cortex. *Proceedings of the National Academy of Sciences of the United States of America*, *106*(42), 18034–18039. https://doi.org/10.1073/pnas.0810943106

Conwell, C., MacMahon, E., Jagadeesh, A., Vinken, K., Sharma, S., Prince, J. S., Alvarez, G. A., Konkle, T., Livingstone, M., & Isik, L. (2025). *Monkey See, Model Knew: Large Language Models Accurately Predict Visual Brain Responses in Humans* and *Non-Human Primates*. https://doi.org/10.1101/2025.03.05.641284

Delacre, M., Lakens, D., & Leys, C. (2017). Why psychologists should by default use welch's t-Test instead of student's t-Test. *International Review of Social Psychology*, *30*(1), 92–101. https://doi.org/10.5334/irsp.82

Devlin, J. T., Rushworth, M. F. S., & Matthews, P. M. (2005). Category-related activation for written words in the posterior fusiform is task specific. *Neuropsychologia*, *43*(1), 69–74. https://doi.org/10.1016/j.neuropsychologia.2004.06.013

Dijkstra, N., Bosch, S. E., & van Gerven, M. A. J. (2017). Vividness of visual imagery depends on the neural overlap with perception in visual areas. *Journal of Neuroscience*, *37*(5), 1367–1373. https://doi.org/10.1523/JNEUROSCI.3022-16.2016

Fang, F., & He, S. (2005). Cortical responses to invisible objects in the human dorsal and ventral pathways. *Nature Neuroscience*, *8*(10), 1380–1385. https://doi.org/10.1038/nn1537

Favila, S. E., Kuhl, B. A., & Winawer, J. (2022). Perception and memory have distinct spatial tuning properties in human visual cortex. *Nature Communications*, *13*(1), 5864. https://doi.org/10.1038/s41467-022-33161-8

Harrison, S. A., & Tong, F. (2009). Decoding reveals the contents of visual working memory in early visual areas. *Nature*, *458*(7238), 632–635. https://doi.org/10.1038/nature07832

He, C., Peelen, M. V., Han, Z., Lin, N., Caramazza, A., & Bi, Y. (2013). Selectivity for large nonmanipulable objects in scene-selective visual cortex does not require visual experience. *NeuroImage*, *79*, 1–9. https://doi.org/10.1016/j.neuroimage.2013.04.051

Hendriks, M. H. A., Daniels, N., Pegado, F., & de Beeck, H. P. O. (2017). The effect of spatial smoothing on representational similarity in a simple motor paradigm. *Frontiers in Neurology*, *8*(MAY), 1–11. https://doi.org/10.3389/fneur.2017.00222

Hsu, N. S., Kraemer, D. J. M., Oliver, R. T., Schlichting, M. L., & Thompson-Schill, S. L. (2011). Color, Context, and Cognitive Style: Variations in Color Knowledge Retrieval as a Function of Task and

Subject Variables. *Journal of Cognitive Neuroscience*, *23*(9), 2544–2557. https://doi.org/10.1162/jocn.2011.21619

Kassambara, A. (2021). *rstatix: Pipe-friendly framework for basic statistical tests. R package version 0.7. 0*.

Keogh, R., Bergmann, J., & Pearson, J. (2020). Cortical excitability controls the strength of mental imagery. *ELife*, *9*, 1–33. https://doi.org/10.7554/eLife.50232

Koelsch, S., Schulze, K., Sammler, D., Fritz, T., Müller, K., & Gruber, O. (2009). Functional architecture of verbal and tonal working memory: An FMRI study. *Human Brain Mapping*, *30*(3), 859–873. https://doi.org/10.1002/hbm.20550

Koenigs, M., Barbey, A. K., Postle, B. R., & Grafman, J. (2009). Superior Parietal Cortex Is Critical for the Manipulation of Information in Working Memory. *The Journal of Neuroscience*, *29*(47), 14980–14986. https://doi.org/10.1523/JNEUROSCI.3706-09.2009

Kosslyn, S. M., Ganis, G., & Thompson, W. L. (2001). Neural foundations of imagery. *Nature Reviews Neuroscience*, *2*(9), 635–642. https://doi.org/10.1038/35090055

Kosslyn, S. M., Pascual-Leone, A., Felician, O., Camposano, S., Keenan, J. P., Thompson, W. L., Ganis, G., Sukel, K. E., & Alpert, N. M. (1999). The Role of Area 17 in Visual Imagery : Convergent Evidence from PET and rTMS Published by : American Association for the Advancement of Science Stable URL : http://www.jstor.org/stable/2899164 Linked references are available on JSTOR for this article : T. *Science*, *284*(5411), 167–170.

Kumar, S., Joseph, S., Gander, P. E., Barascud, N., Halpern, A. R., & Griffiths, T. D. (2016). A brain system for auditory working memory. *Journal of Neuroscience*, *36*(16), 4492–4505. https://doi.org/10.1523/JNEUROSCI.4341-14.2016

Lee, S. H., Kravitz, D. J., & Baker, C. I. (2012). Disentangling visual imagery and perception of real-world objects. *NeuroImage*, *59*(4), 4064–4073. https://doi.org/10.1016/j.neuroimage.2011.10.055

Li, S., Zeng, X., Shao, Z., & Yu, Q. (2023). Neural Representations in Visual and Parietal Cortex Differentiate between Imagined, Perceived, and Illusory Experiences. *The Journal of Neuroscience*, *43*(38), 6508–6524. https://doi.org/10.1523/JNEUROSCI.0592-23.2023

Liu, B., Wang, X., Wang, X., Li, Y., Han, Y., Lu, J., Zhang, H., Wang, X., & Bi, Y. (2025). Object knowledge representation in the human visual cortex requires a connection with the language system. *PLOS Biology*, *23*(5). https://doi.org/10.1371/journal.pbio.3003161

Liu, J., & Bartolomeo, P. (2023). Probing the unimaginable: The impact of aphantasia on distinct domains of visual mental imagery and visual perception. *Cortex*, *166*, 338–347. https://doi.org/10.1016/j.cortex.2023.06.003

Liu, J., Zhan, M., Hajhajate, D., Spagna, A., Dehaene, S., Cohen, L., & Bartolomeo, P. (2025). Visual mental imagery in typical imagers and in aphantasia: A millimeter-scale 7-T fMRI study. *Cortex*, *185*, 113–132. https://doi.org/10.1016/j.cortex.2025.01.013

Maclean, M. W., Hadid, V., Spreng, R. N., & Lepore, F. (2023). Revealing robust neural correlates of conscious and unconscious visual processing: Activation likelihood estimation meta-analyses. *NeuroImage*, *273*, 120088. https://doi.org/10.1016/j.neuroimage.2023.120088

Mahon, B. Z., Anzellotti, S., Schwarzbach, J., Zampini, M., & Caramazza, A. (2009). Category-Specific Organization in the Human Brain Does Not Require Visual Experience. *Neuron*, *63*(3), 397–405. https://doi.org/10.1016/j.neuron.2009.07.012

Mahon, B. Z. B. Z., & Caramazza, A. (2011). What drives the organization of object knowledge in the brain? *Trends in Cognitive Sciences*, *15*(3), 97–103. https://doi.org/10.1016/j.tics.2011.01.004

Marks, D. F. (1973). VISUAL IMAGERY DIFFERENCES IN THE RECALL OF PICTURES. *British Journal of Psychology*, *64*(1), 17–24. https://doi.org/10.1111/j.2044-8295.1973.tb01322.x

Martin, A. (2007). The Representation of Object Concepts in the Brain. *Annual Review of Psychology*, *58*(1), 25–45. https://doi.org/10.1146/annurev.psych.57.102904.190143

Martin, A. (2016). GRAPES—Grounding representations in action, perception, and emotion systems: How object properties and categories are represented in the human brain. *Psychonomic Bulletin and Review*, *23*(4), 979–990. https://doi.org/10.3758/s13423-015-0842-3

Martin, A., Wiggs, C. L., Ungerleider, L. G., & Haxby, J. V. (1996). Neural correlates of category-specific knowledge. *Nature*, *379*(6566), 649–652. https://doi.org/10.1038/379649a0

Montabes de la Cruz, B. M., Abbatecola, C., Luciani, R. S., Paton, A. T., Bergmann, J., Vetter, P., Petro, L. S., & Muckli, L. F. (2024). Decoding sound content in the early visual cortex of aphantasic participants. *Current Biology*. https://doi.org/10.1016/j.cub.2024.09.008

Nalborczyk, L. (2025, January 7). *Making Sense of Commonality Analysis*. https://lnalborczyk.github.io/blog/2025-01-07-commonality

Op de Beeck, H. P. (2010). Against hyperacuity in brain reading: Spatial smoothing does not hurt multivariate fMRI analyses? *NeuroImage*, *49*(3), 1943–1948. https://doi.org/10.1016/j.neuroimage.2009.02.047

Paivio, A. (1991). Dual coding theory: Retrospect and current status. *Canadian Journal of Psychology/Revue Canadienne de Psychologie*, *45*(3), 255.

Pearson, J. (2019). The human imagination: the cognitive neuroscience of visual mental imagery. *Nature Reviews Neuroscience*, *20*(10), 624–634. https://doi.org/10.1038/s41583-019-0202-9

Pearson, J. (2020). Reply to: Assessing the causal role of early visual areas in visual mental imagery. *Nature Reviews Neuroscience*, *21*(9), 517–518. https://doi.org/10.1038/s41583-020-0349-4

Pearson, J., & Kosslyn, S. M. (2015). The heterogeneity of mental representation: Ending the imagery debate. *Proceedings of the National Academy of Sciences*, *112*(33), 10089–10092. https://doi.org/10.1073/pnas.1504933112

Peelen, M. V. M. V., Bracci, S., Lu, X., He, C., Caramazza, A., & Bi, Y. (2013). Tool selectivity in left occipitotemporal cortex develops without vision. *Journal of Cognitive Neuroscience*, *25*(8), 1225–1234. https://doi.org/10.1162/jocn_a_00411

Peelen, M. V., He, C., Han, Z., Caramazza, A., & Bi, Y. (2014). Nonvisual and Visual Object Shape Representations in Occipitotemporal Cortex: Evidence from Congenitally Blind and Sighted Adults. *The Journal of Neuroscience*, *34*(1), 163–170. https://doi.org/10.1523/JNEUROSCI.1114-13.2014

R Core Team. (2019). *R: A language and environment for statistical computing. R Foundation for Statistical Computing, Vienna, Austria*. *3*. https://www.r-project.org/

Radford, A., Kim, J. W., Hallacy, C., Ramesh, A., Goh, G., Agarwal, S., Sastry, G., Askell, A., Mishkin, P., Clark, J., Krueger, G., & Sutskever, I. (2021). *Learning Transferable Visual Models From Natural Language Supervision*. http://arxiv.org/abs/2103.00020

Schneiders, J. A., Opitz, B., Tang, H., Deng, Y., Xie, C., Li, H., & Mecklinger, A. (2012). The impact of auditory working memory training on the fronto-parietal working memory network. *Frontiers in Human Neuroscience*, *JUNE 2012*. https://doi.org/10.3389/fnhum.2012.00173

Shivde, G., & Thompson-Schill, S. L. (2004). Dissociating semantic and phonological maintenance using fMRI. *Cognitive, Affective, & Behavioral Neuroscience*, *4*(1), 10–19. https://doi.org/10.3758/CABN.4.1.10

Shoham, A., Grosbard, I. D., Patashnik, O., Cohen-Or, D., & Yovel, G. (2024). Using deep neural networks to disentangle visual and semantic information in human perception and memory. *Nature Human Behaviour*, *8*(4), 702–717. https://doi.org/10.1038/s41562-024-01816-9

Spagna, A., Hajhajate, D., Liu, J., & Bartolomeo, P. (2021). Visual mental imagery engages the left fusiform gyrus, but not the early visual cortex: A meta-analysis of neuroimaging evidence. *Neuroscience and Biobehavioral Reviews*, *122*(December 2020), 201–217. https://doi.org/10.1016/j.neubiorev.2020.12.029

Spagna, A., Heidenry, Z., Miselevich, M., Lambert, C., Eisenstadt, B. E., Tremblay, L., Liu, Z., Liu, J., & Bartolomeo, P. (2024). Visual mental imagery: Evidence for a heterarchical neural architecture. *Physics of Life Reviews*, *48*(December 2023), 113–131. https://doi.org/10.1016/j.plrev.2023.12.012

Suzuki, M., Noguchi, Y., & Kakigi, R. (2014). Temporal dynamics of neural activity underlying unconscious processing of manipulable objects. *Cortex*, *50*, 100–114. https://doi.org/10.1016/j.cortex.2013.09.005

Uluç, I., Schmidt, T. T., Wu, Y. hao, & Blankenburg, F. (2018). Content-specific codes of parametric auditory working memory in humans. *NeuroImage*, *183*, 254–262. https://doi.org/10.1016/j.neuroimage.2018.08.024

Valente, G., Castellanos, A. L., Hausfeld, L., De Martino, F., & Formisano, E. (2021). Cross-validation and permutations in MVPA: Validity of permutation strategies and power of cross-validation schemes. *NeuroImage*, *238*. https://doi.org/10.1016/j.neuroimage.2021.118145

van den Hurk, J., Van Baelen, M., & Op de Beeck, H. P. (2017). Development of visual category selectivity in ventral visual cortex does not require visual experience. *Proceedings of the National Academy of Sciences*, *114*(22), E4501–E4510. https://doi.org/10.1073/pnas.1612862114

Vetter, P., Bola, Ł., Reich, L., Bennett, M., Muckli, L., & Amedi, A. (2020). Decoding Natural Sounds in Early “Visual” Cortex of Congenitally Blind Individuals. *Current Biology*, *30*(15), 3039-3044.e2. https://doi.org/10.1016/j.cub.2020.05.071

Vetter, P., Smith, F. W., & Muckli, L. (2014). Decoding sound and imagery content in early visual cortex. *Current Biology*, *24*(11), 1256–1262. https://doi.org/10.1016/j.cub.2014.04.020

Wang, A. Y., Kay, K., Naselaris, T., Tarr, M. J., & Wehbe, L. (2023). Better models of human high-level visual cortex emerge from natural language supervision with a large and diverse dataset. *Nature Machine Intelligence*, *5*(12), 1415–1426. https://doi.org/10.1038/s42256-023-00753-y

Wang, X., Men, W., Gao, J., Caramazza, A., & Bi, Y. (2020). Two Forms of Knowledge Representations in the Human Brain. *Neuron*, *107*(2), 1–11. https://doi.org/10.1016/j.neuron.2020.04.010

Willenbockel, V., Sadr, J., Fiset, D., Horne, G. O., Gosselin, F., & Tanaka, J. W. (2010). Controlling low-level image properties: The SHINE toolbox. *Behavior Research Methods*, *42*(3), 671–684. https://doi.org/10.3758/BRM.42.3.671

Wurm, M. F., & Caramazza, A. (2019). Lateral occipitotemporal cortex encodes perceptual components of social actions rather than abstract representations of sociality. *NeuroImage*, *202*. https://doi.org/10.1016/j.neuroimage.2019.116153

Wurm, M. F., & Caramazza, A. (2022). Two ‘what’ pathways for action and object recognition. *Trends in Cognitive Sciences*, *26*(2), 103–116. https://doi.org/10.1016/j.tics.2021.10.003

Xu, Y. (2018). The Posterior Parietal Cortex in Adaptive Visual Processing. *Trends in Neurosciences*, *41*(11), 806–822. https://doi.org/10.1016/j.tins.2018.07.012

Xu, Y., & Chun, M. M. (2006). Dissociable neural mechanisms supporting visual short-term memory for objects. *Nature*, *440*(7080), 91–95. https://doi.org/10.1038/nature04262

Xu, Y., Vignali, L., Sigismondi, F., Crepaldi, D., Bottini, R., & Collignon, O. (2023). Similar object shape representation encoded in the inferolateral occipitotemporal cortex of sighted and early blind people. *PLOS Biology*, *21*(7), e3001930. https://doi.org/10.1371/journal.pbio.3001930

Yang, A., Pan, J., Lin, J., Men, R., Zhang, Y., Zhou, J., & Zhou, C. (2023). *Chinese CLIP: Contrastive Vision-Language Pretraining in Chinese*. http://arxiv.org/abs/2211.01335

Zeman, A. (2024). Aphantasia and hyperphantasia: exploring imagery vividness extremes. *Trends in Cognitive Sciences*, *28*(5), 467–480. https://doi.org/10.1016/j.tics.2024.02.007

Zeman, A., Dewar, M., & Della Sala, S. (2015). Lives without imagery – Congenital aphantasia. *Cortex*, *73*, 378–380. https://doi.org/10.1016/j.cortex.2015.05.019

Figures

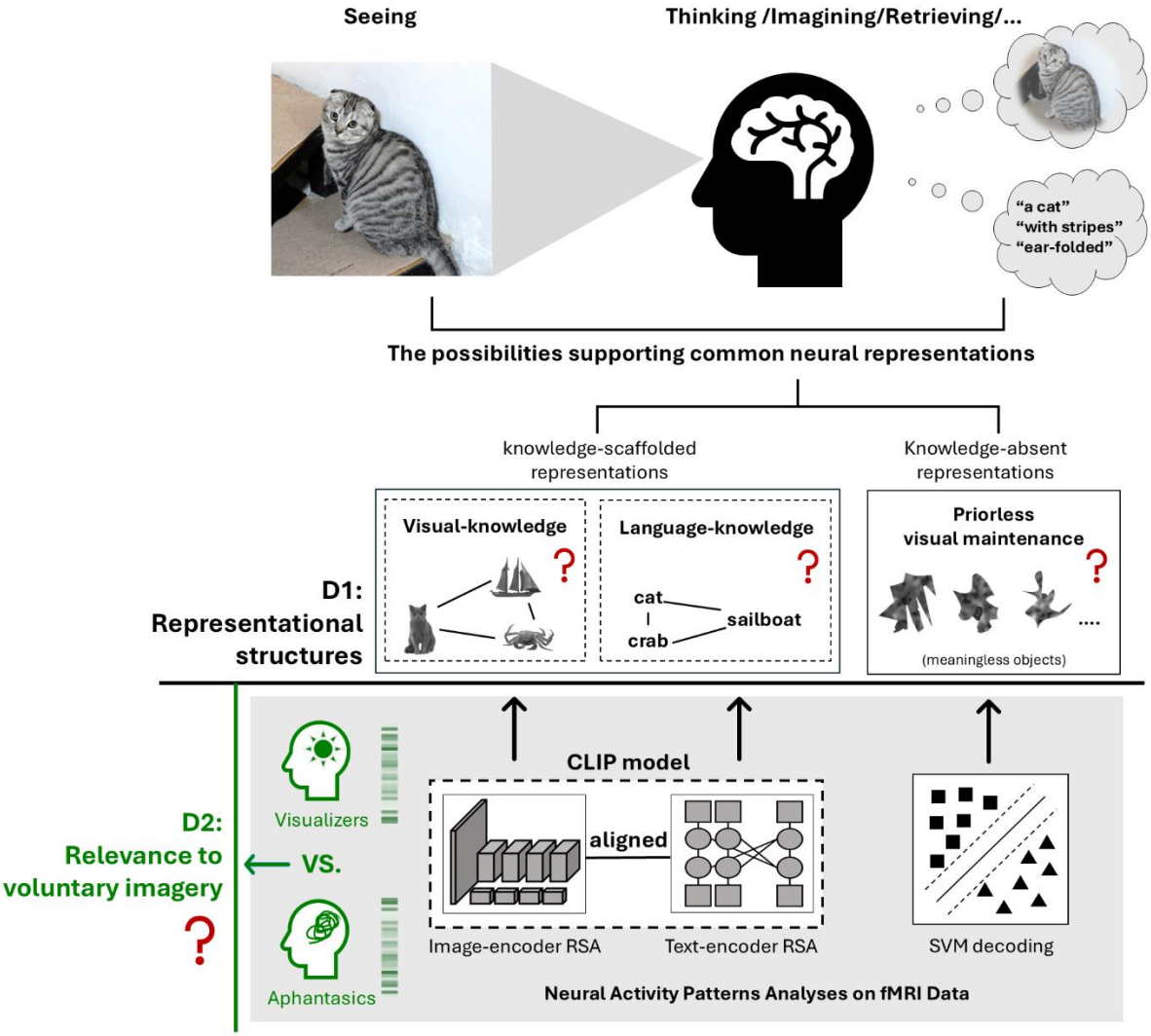

Fig. 1 | Hypotheses framework. We hypothesized that multiple representational mechanisms contribute to shared neural representations across the presence and absence of visual input, and tested the mechanisms along two key dimensions: **D1-representational structures**, including visual-knowledge representation, language-knowledge representation, and priorless visual maintenance representation. **D2-voluntary imagery relevance**. D1 was assessed through the combination of cross-decoding and multimodal deep neural network (DNN) model RSA; and D2 was assessed via group comparisons between participants with and without conscious visual imagery experience (i.e., visualizers vs. aphantasics).

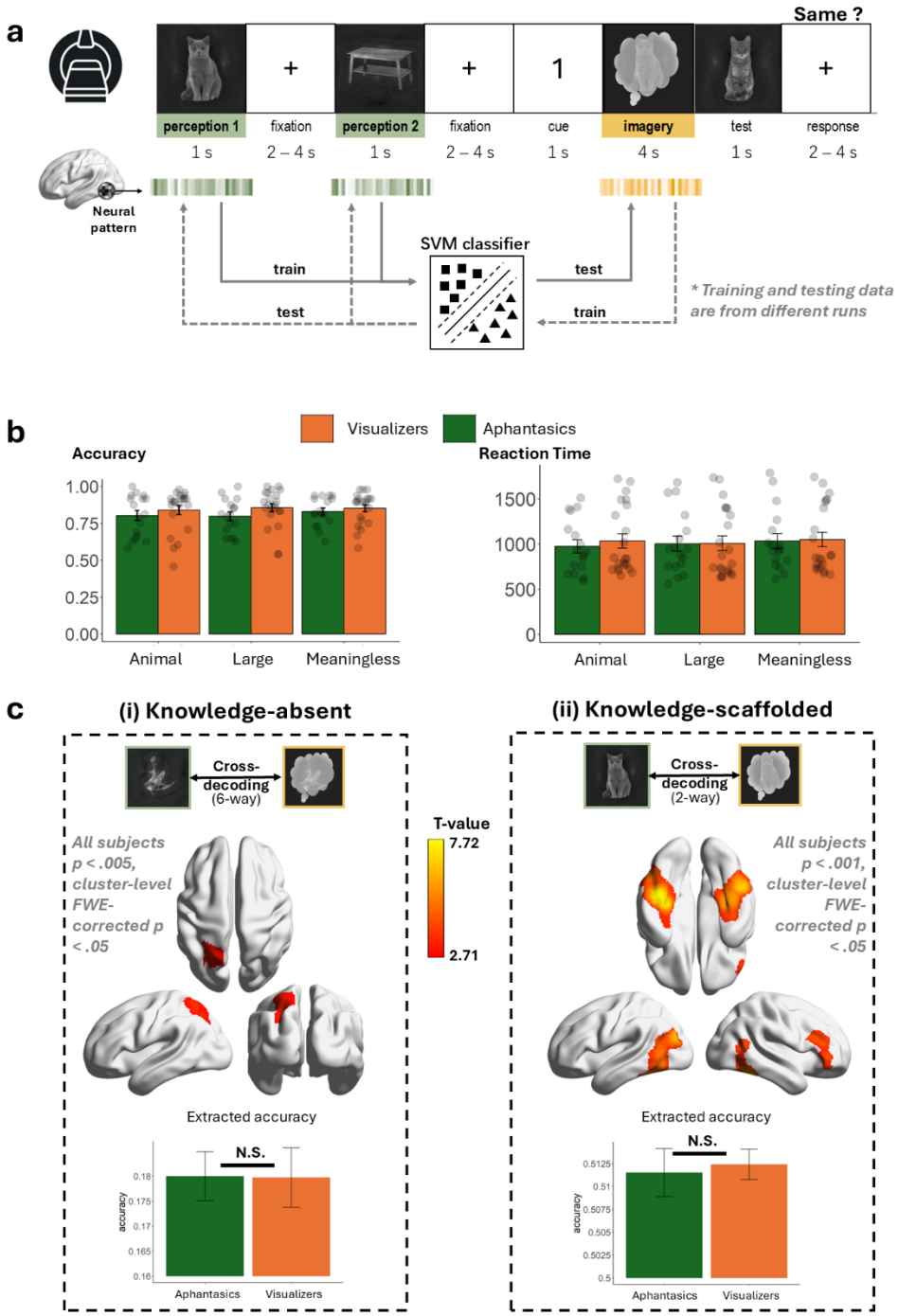

Fig. 2 | Experimental design, behavioral performance, and cross-decoding results. a, Schematic of the fMRI experiment and cross-modal SVM decoding. A retro-cue paradigm was used during scanning. Each trial began with sequential presentation of two images (perception phase), followed by a numeric cue indicating which image to visualize (imagery phase). A test image was then presented, and participants judged whether it was exactly the same image (not just the same object) as the cued one. SVM decoding was performed across perception and imagery phases from different runs using a repeated split-half

cross-validation approach (see 'Searchlight SVM Decoding Analysis' in Methods for details). **b**, Behavioral performance. Bar plots show mean accuracy and reaction times (RTs) for each group, with error bars representing ±1 SEM. Dots indicate individual participant data. **c**, Searchlight SVM cross-decoding results. (i) Six-way item-level decoding map of meaningless shapes (voxelwise $p < .005$, cluster-level FWE-corrected $p < .05$). (ii) Two-way object domain-level decoding map (voxelwise $p < .001$, cluster-level FWE-corrected $p < .05$). Full item-level results are provided in Supplementary Fig. 4. Bar plots display the mean accuracy extracted from the significant clusters shown above for each group, with error bars representing ±1 SEM.

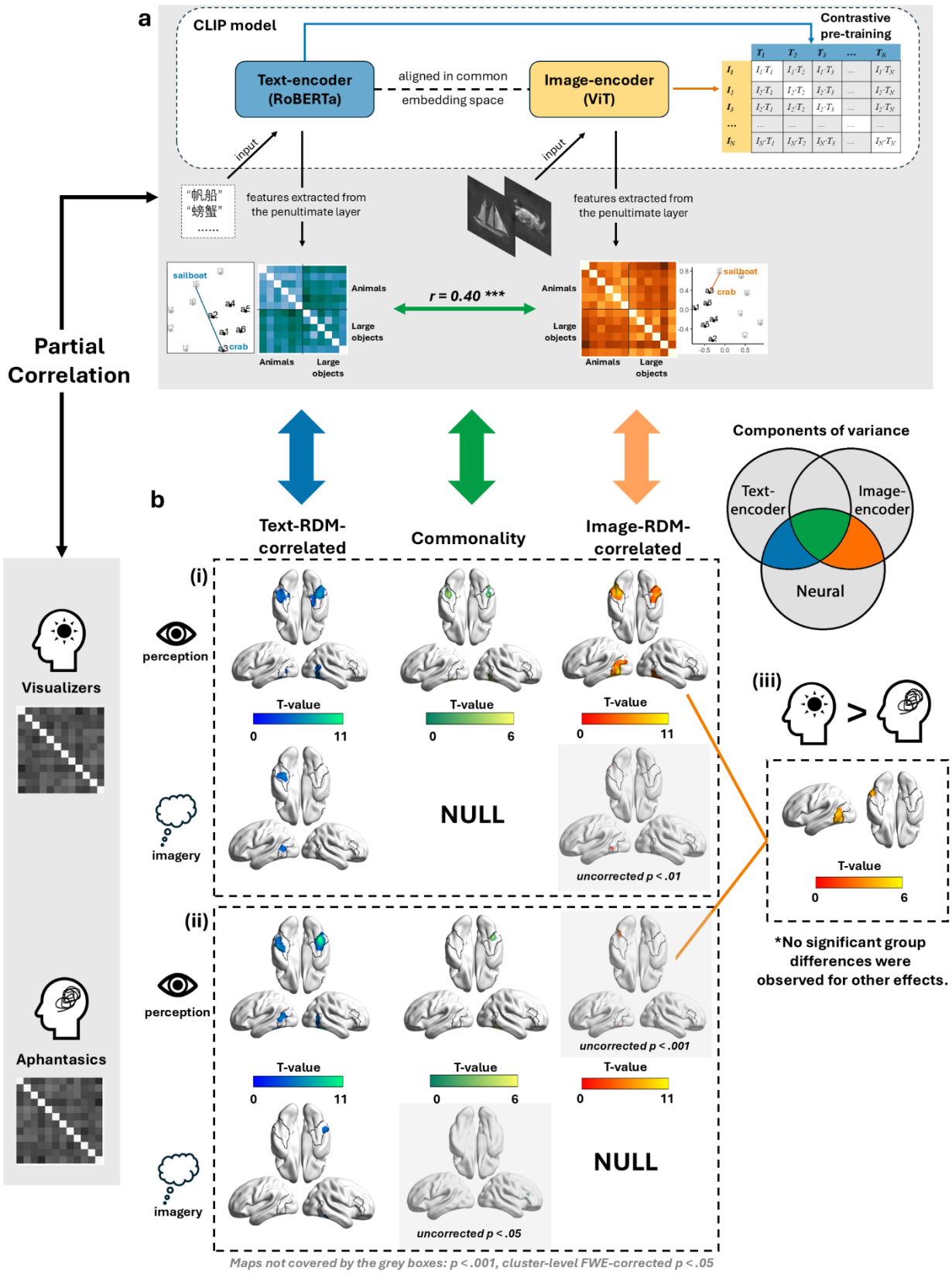
a
CLIP model
Contrastive pre-training
Text-encoder (RoBERTa)
aligned in common embedding space
Image-encoder (ViT)
input
"帆船"
"螃蟹"
.....
features extracted from the penultimate layer
features extracted from the penultimate layer
sailboat
crab
Animals
Large objects
r = 0.40 ***
Partial Correlation
b
Text-RDM-correlated
Commonality
Image-RDM-correlated
Components of variance
Text-encoder
Image-encoder
Neural
(i)
perception
imagery
T-value
0
11
6
NULL
uncorrected p < .01
(ii)
uncorrected p < .001
uncorrected p < .05
(iii)
*No significant group differences were observed for other effects.
Visualizers
Aphantasics
Maps not covered by the grey boxes: p < .001, cluster-level FWE-corrected p < .05

F**ig. 3 | Searchlight RSA with CLIP encoders. a**, We used a multimodal deep neural network—Contrastive Language-Image Pre-Training (CLIP, Chinese version)—to examine neural representational structures. It jointly trains an image-encoder and a text-encoder to align images and their corresponding textual descriptions in a shared embedding space using contrastive learning. Stimulus labels were input into the text-encoder and stimulus images into the image-encoder; embeddings from the penultimate layer were used to compute representational dissimilarity matrices (RDMs) based on cosine distance. Although the RDMs from the image and text encoders were significantly correlated ($r = 0.40$, $p < .001$), they captured distinct representational properties. For example, "sailboat" and "crab" were farther apart in the text embedding space but closer together in the visual embedding space. Searchlight RSA was conducted within the mask showing significant cross-decoding for real object domains (from Fig. 2c-ii), which was demarcated by black boundaries on the brain maps. For each searchlight sphere, we computed partial correlations between the neural RDM and one encoder RDM while controlling for the other, as well as the shared variance (commonality) between the neural RDM and the two encoder RDMs. **b**, Searchlight RSA results. Blue regions show significant partial correlations with the text-RDM; orange-red regions show significant partial correlations with the image-RDM; green regions show significant commonality across neural-, image-, and text-RDMs. The Venn diagram indicates the components of variance. (i) results in the visualizer group; (ii) results in the aphantasic group; (iii) regions showing significant group differences, observed only in the partial correlations between neural- and image-RDM during the perception phase. Maps not covered by the grey boxes are thresholded at voxelwise $p < .001$, cluster-level FWE-corrected $p < .05$. Maps within the grey boxes did not survive multiple-comparisons correction and are displayed at the most stringent threshold they reached. All uncorrected results are shown in Supplementary Fig. 6.

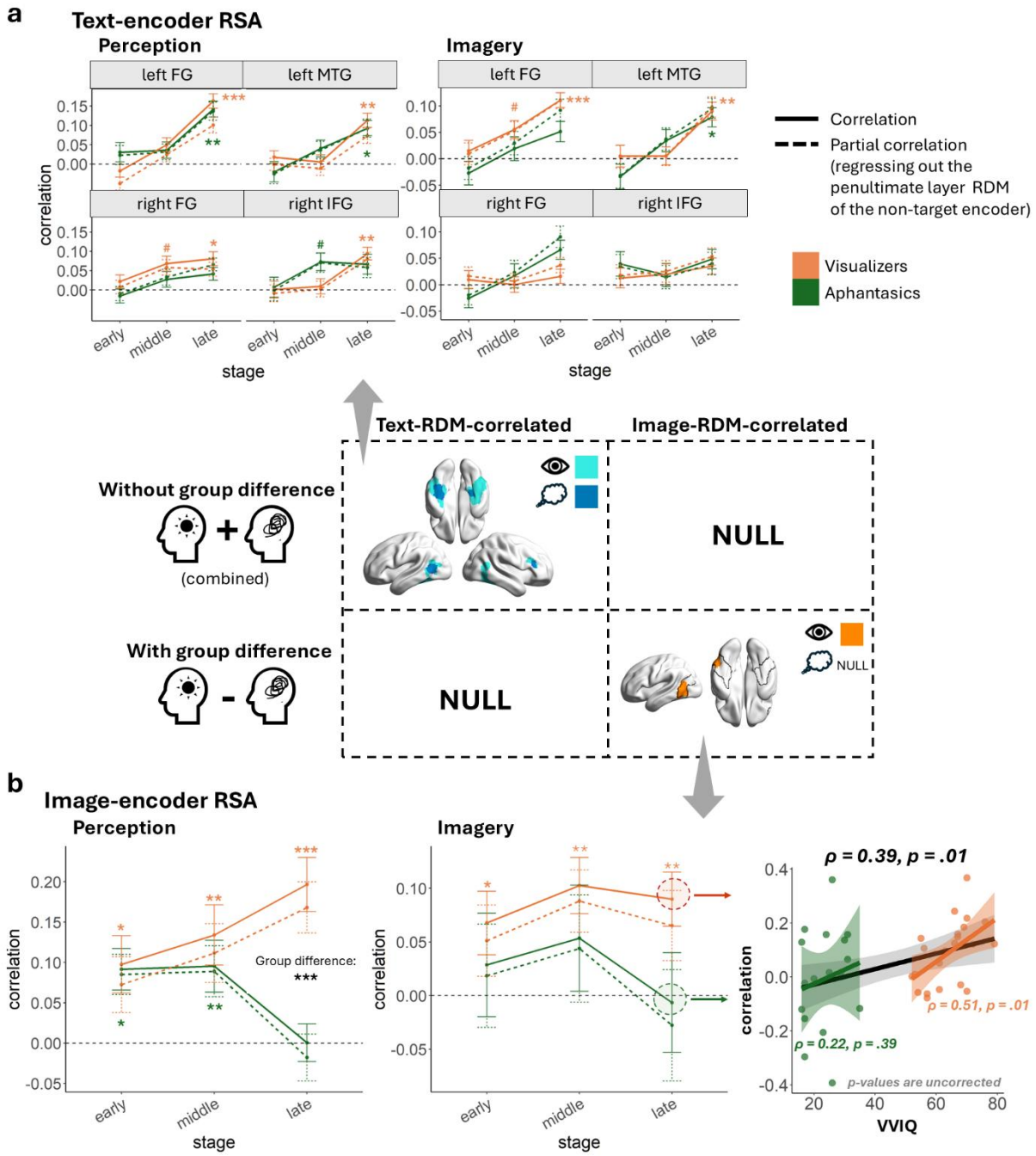

Fig. 4 | ROI-based RSA with different processing hierarchies of the CLIP model. Two types of regions of interest (ROIs) were defined based on searchlight RSA results: the **language-knowledge-imagery-irrelevant ROIs** were defined as the overlap of regions showing significant similarity to the text-RDM in the group-level analysis combining all subjects across both the perception and imagery phases (see statistical maps in Supplementary Fig. 5); the **visual-knowledge-imagery-relevant ROI** was defined as the region showing significant group differences in similarity to the image-RDM, which was only observed during the perception phase in the searchlight analysis. **a**, The layers of the text-encoder were

grouped into three parts: early (layers 1-4), middle (5-8), and late (9-12). Correlations (solid lines) and partial correlations (dashed lines) were computed using RDMs from all layers and were averaged within each layer-group. Partial correlations were computed while regressing out the penultimate-layer RDM of the image-encoder. **b**, The layers of the image-encoder were grouped as early (layers 1–8), middle (9–16), and late (17–24). Partial correlations were computed while regressing out the penultimate-layer RDM of the text-encoder. The right panel shows the correlations between VVIQ scores and the mean correlations of the late layers across all subjects (black line), aphantasics (green line), and visualizers (orange line). Asterisks and pound sign indicate different significance levels of correlations: #$p < .1$, *$p < .05$, **$p < .01$, ***$p < .001$. All statistical tests shown were FDR-corrected, except for the right panel in **b**.

Hypotheses		D2: Voluntary-imagery-relevance	
		imagery-relevant	imagery-irrelevant
D1: Representational structures	Visual-structured knowledge	left LOTC	—
	Language-structured knowledge	—	left dorsal LOTC bilateral FG right IFG
	Priorless visual maintenance	—	left SPL

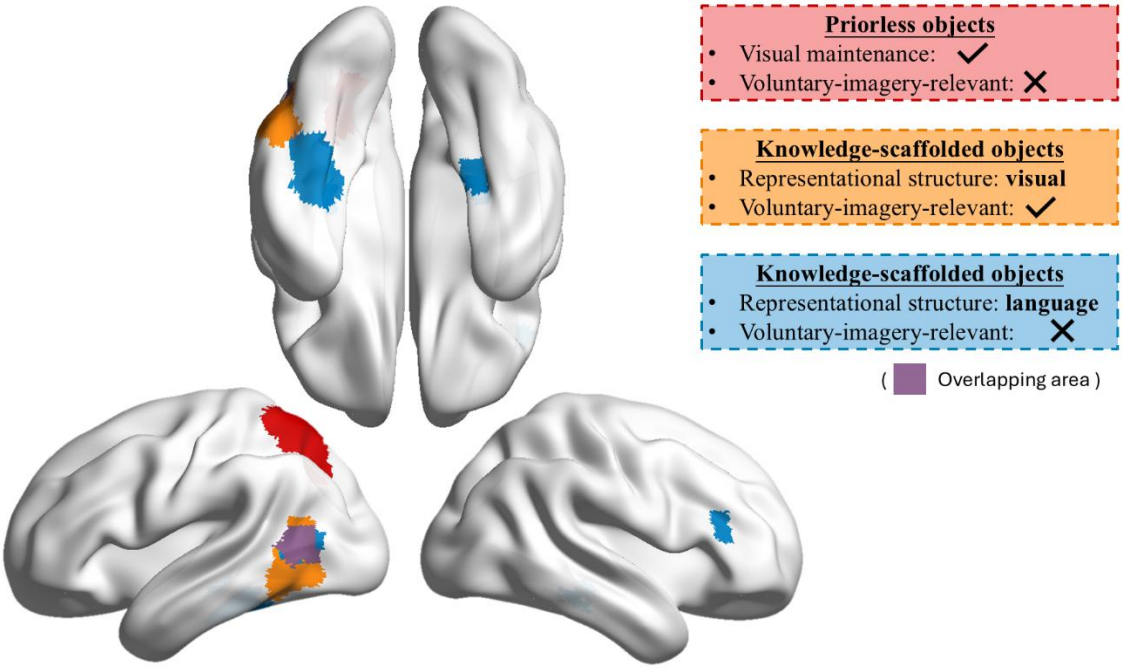

Fig. 5 | Summary of results mapped onto hypothesis framework. The results reveal distinct brain regions supporting shared neural representations across perception and imagery, each associated with specific representational structures: The left LOTC (orange) encodes visual-structured knowledge representation that is sensitive to voluntary imagery experience. The bilateral FG, left dorsal LOTC, and right IFG (blue) encode language-structured knowledge representation that is irrelevant to imagery experience. The left SPL (red) supports priorless visual representation that is unaffected by imagery experience. Purple indicates overlapping area.

Hypotheses		D2: Voluntary-imagery-relevance	
		imagery-relevant	imagery-irrelevant
D1: Representational structures	Visual-structured knowledge	left LOTC	—
	Language-structured knowledge	—	left dorsal LOTC bilateral FG right IFG
	Priorless visual maintenance	—	left SPL

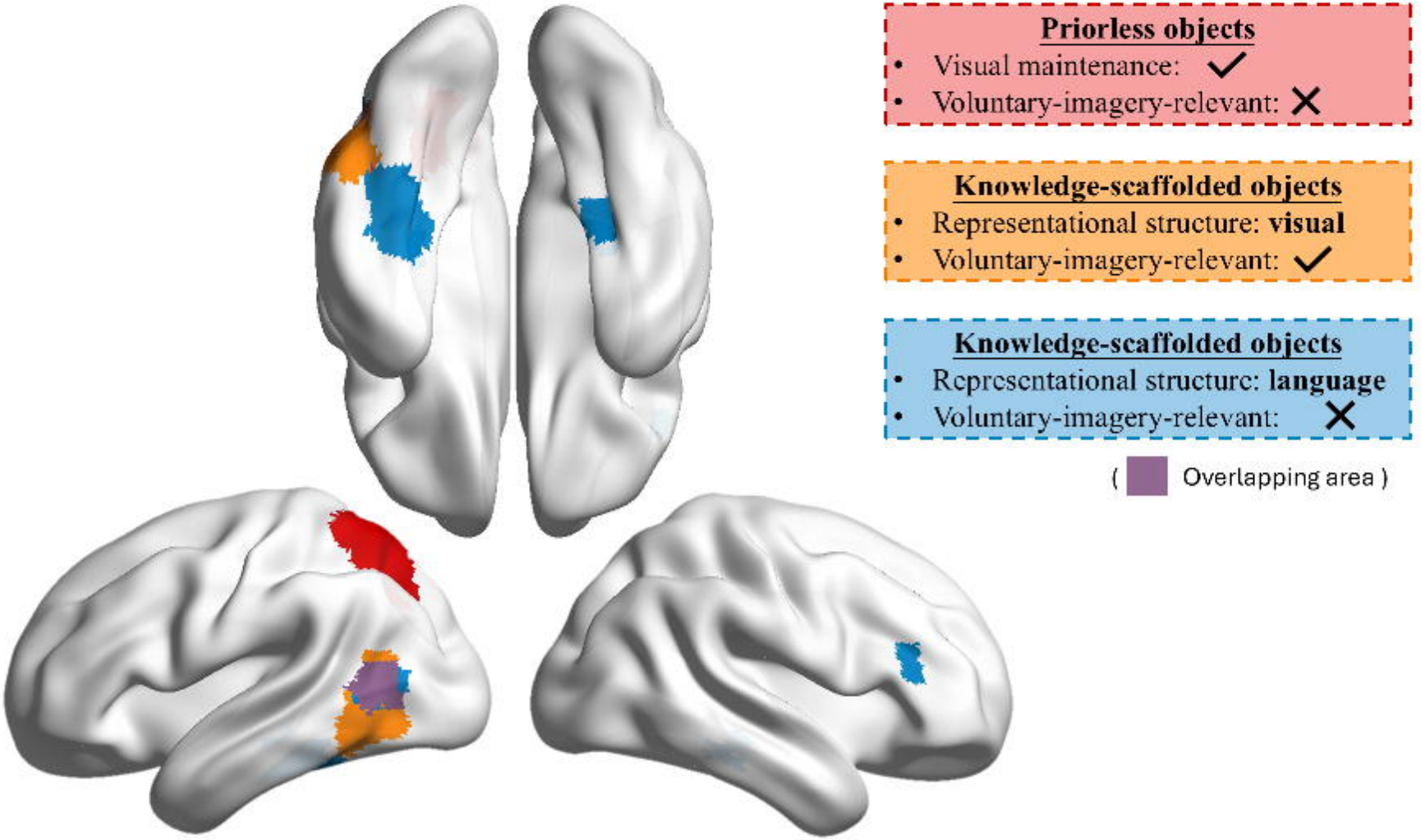

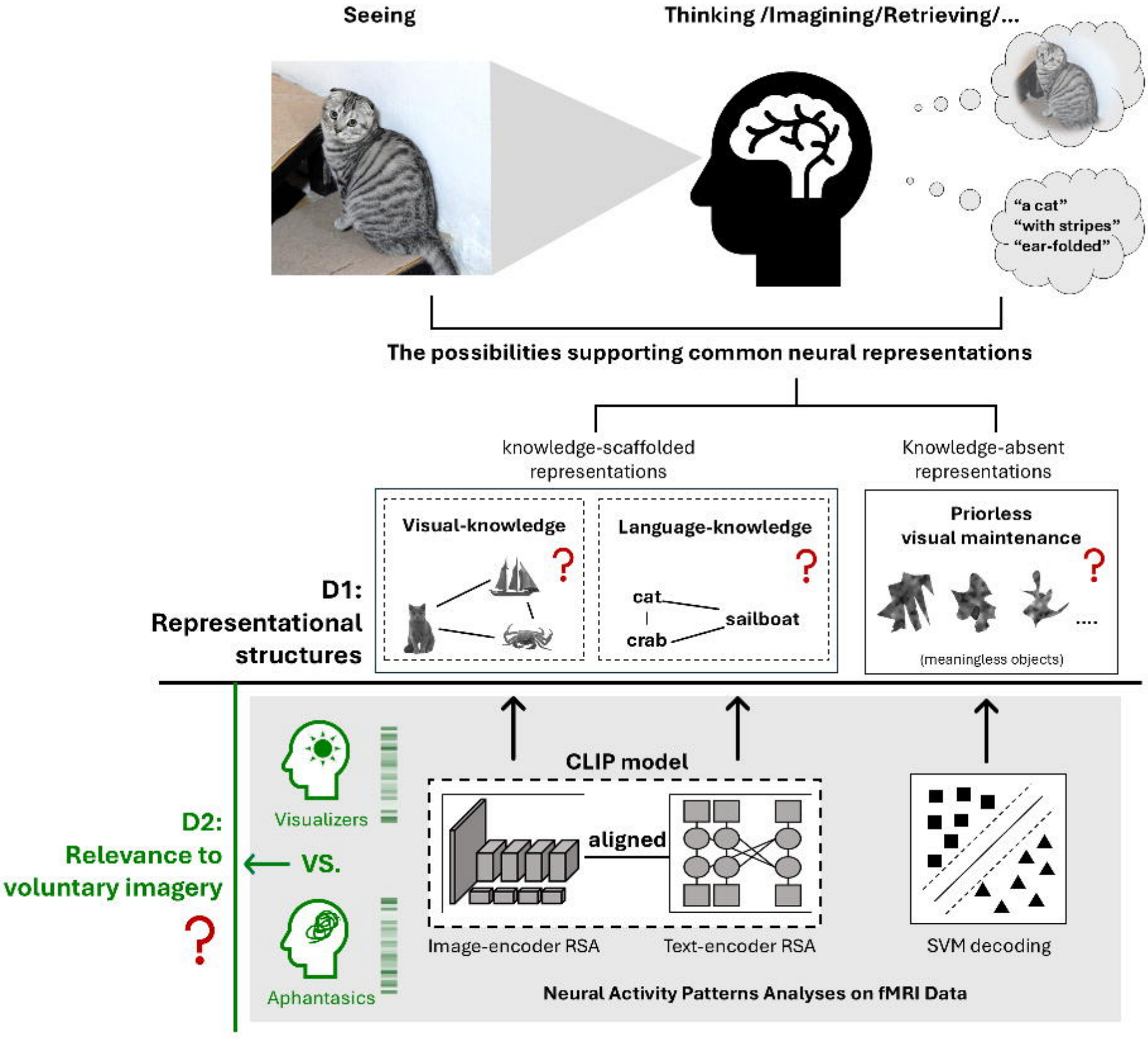
Seeing
Thinking /Imagining/Retrieving/...
"a cat"
"with stripes"
"ear-folded"
The possibilities supporting common neural representations
knowledge-scaffolded representations
Knowledge-absent representations
D1: Representational structures
Visual-knowledge
Language-knowledge
cat
sailboat
crab
Priorless visual maintenance
....
(meaningless objects)
D2: Relevance to voluntary imagery
Visualizers
VS.
Aphantasics
CLIP model
aligned
Image-encoder RSA
Text-encoder RSA
SVM decoding
Neural Activity Patterns Analyses on fMRI Data

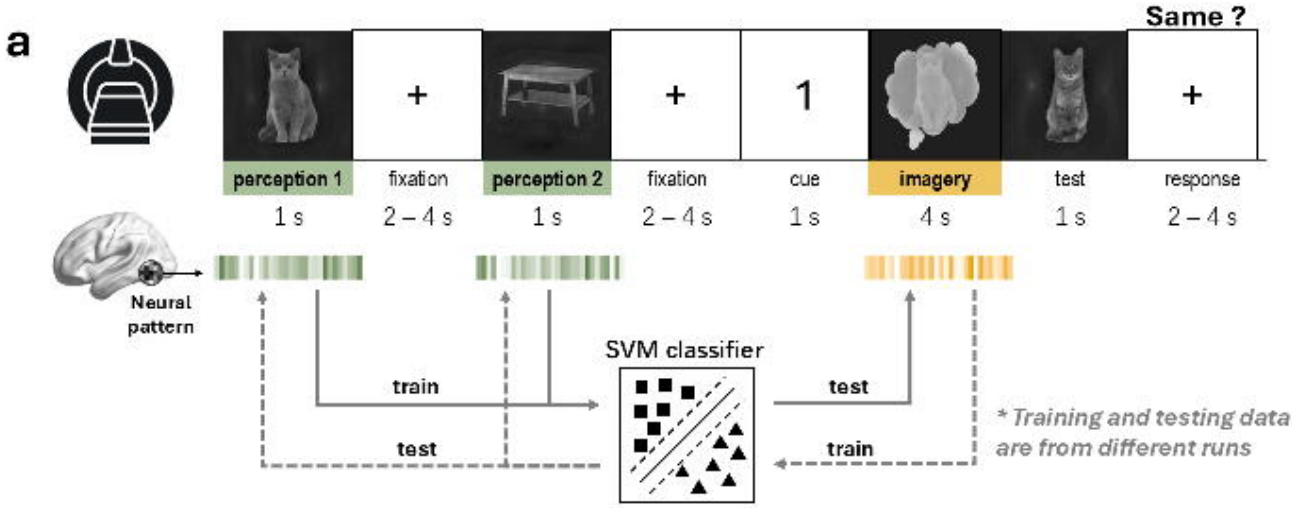
a
Same ?
+
+
1
+
perception 1
fixation
perception 2
fixation
cue
imagery
test
response
1 s
2 – 4 s
1 s
2 – 4 s
1 s
4 s
1 s
2 – 4 s
Neural pattern
SVM classifier
train
test
test
train
* Training and testing data are from different runs

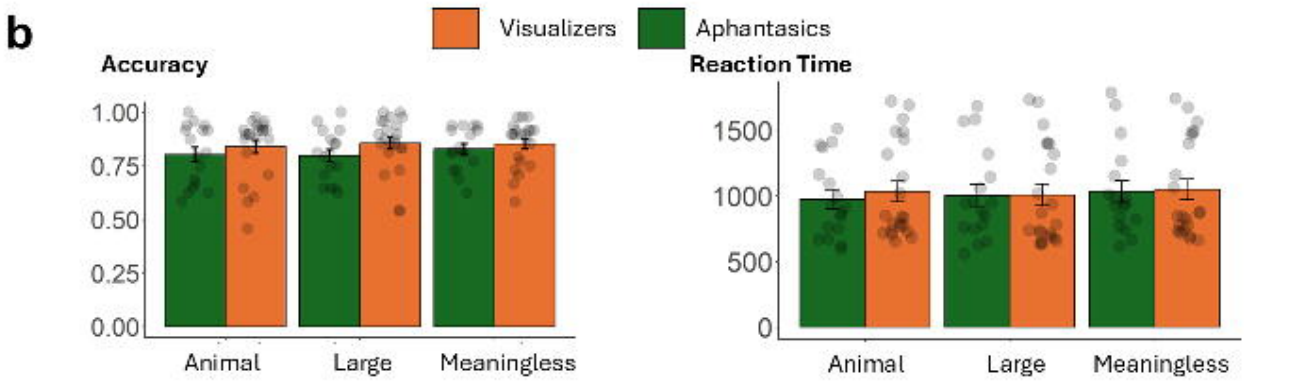
b
Visualizers
Aphantasics
Accuracy
1.00
0.75
0.50
0.25
0.00
Animal
Large
Meaningless
Reaction Time
1500
1000
500
0
Animal
Large
Meaningless

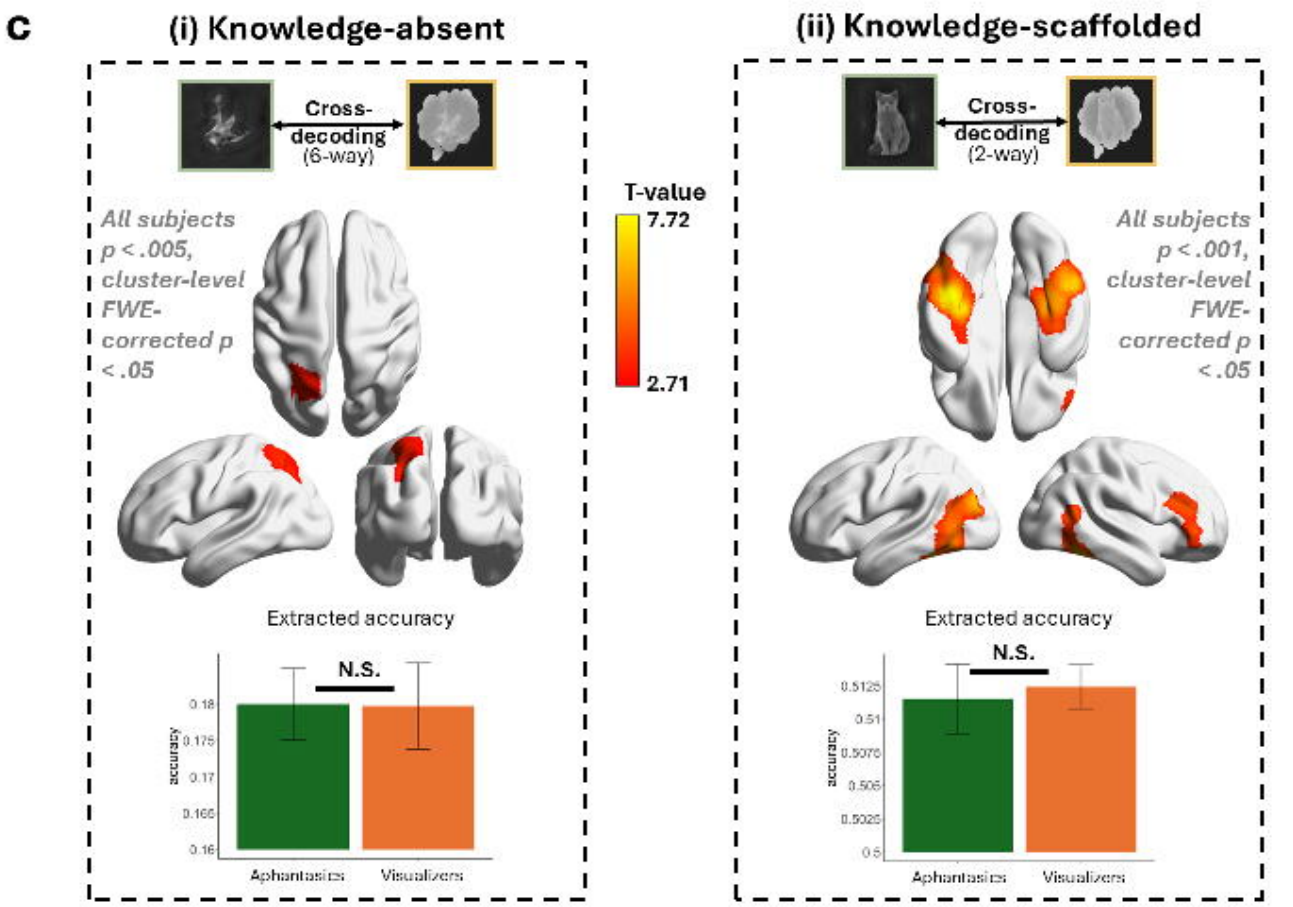
c
(i) Knowledge-absent
Cross-decoding (6-way)
All subjects p < .005, cluster-level FWE-corrected p < .05
T-value
7.72
2.71
Extracted accuracy
N.S.
accuracy
Aphantasics
Visualizers
(ii) Knowledge-scaffolded
Cross-decoding (2-way)
All subjects p < .001, cluster-level FWE-corrected p < .05
Extracted accuracy
N.S.
accuracy
Aphantasics
Visualizers

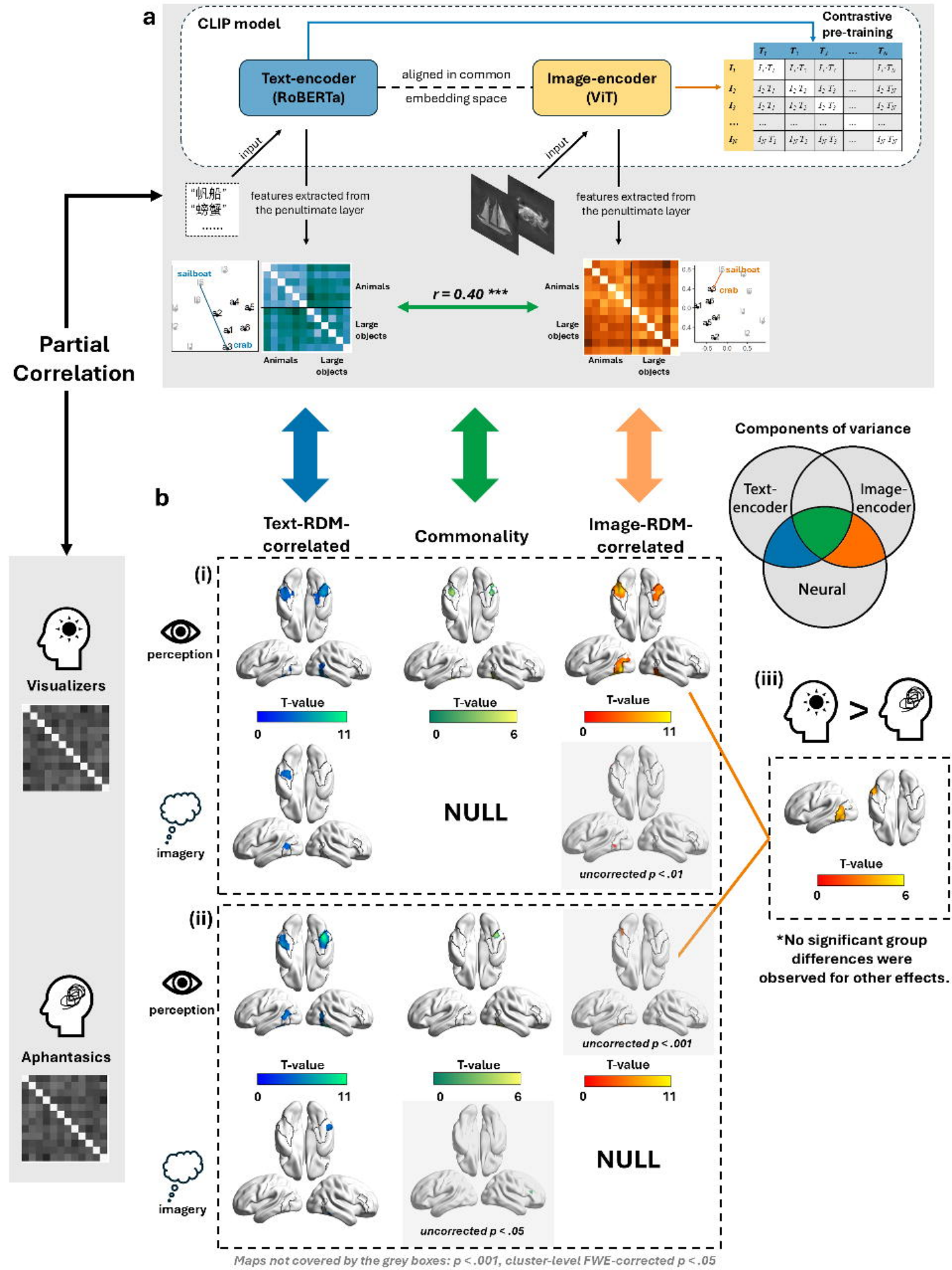
a
CLIP model
Contrastive pre-training
Text-encoder (RoBERTa)
aligned in common embedding space
Image-encoder (ViT)
input
"帆船"
"螃蟹"
.....
features extracted from the penultimate layer
features extracted from the penultimate layer
sailboat
crab
Animals
Large objects
r = 0.40 ***
Partial Correlation
b
Text-RDM-correlated
Commonality
Image-RDM-correlated
Components of variance
Text-encoder
Image-encoder
Neural
(i)
perception
imagery
T-value
0
11
6
NULL
uncorrected p < .01
(ii)
uncorrected p < .001
uncorrected p < .05
(iii)
*No significant group differences were observed for other effects.
Visualizers
Aphantasics
Maps not covered by the grey boxes: p < .001, cluster-level FWE-corrected p < .05

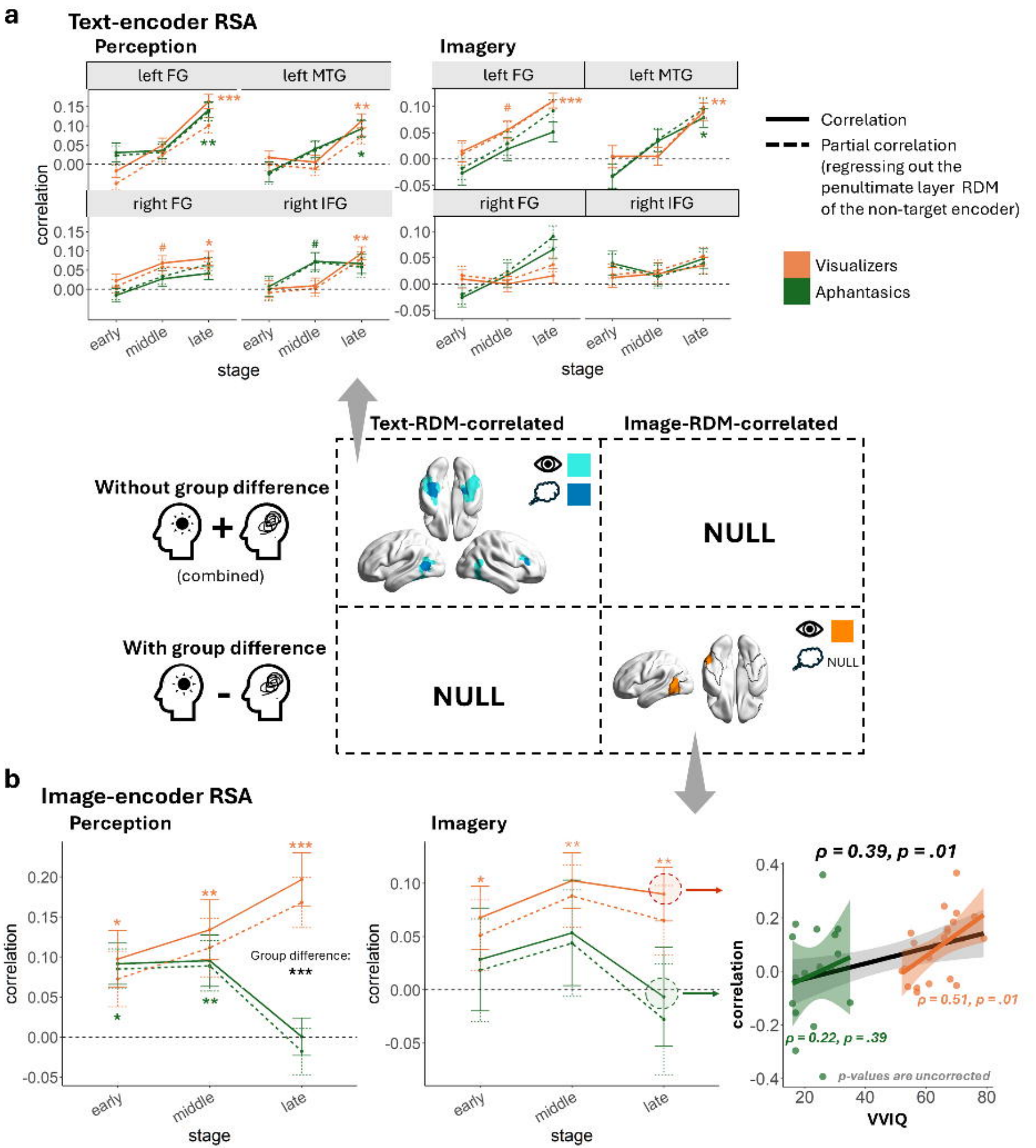
a
Text-encoder RSA
Perception
Imagery
left FG
left MTG
right FG
right IFG
correlation
stage
early
middle
late
Correlation
Partial correlation (regressing out the penultimate layer RDM of the non-target encoder)
Visualizers
Aphantasics
Text-RDM-correlated
Image-RDM-correlated
Without group difference
(combined)
With group difference
NULL
NULL
NULL
b
Image-encoder RSA
Perception
Imagery
Group difference: ***
ρ = 0.39, p = .01
ρ = 0.51, p = .01
ρ = 0.22, p = .39
p-values are uncorrected
VVIQ